





























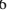


Discovery of Ancient Globular Cluster Candidates in The Relic, a Quiescent Galaxy at $z=2.5$

KATHERINE E. WHITAKER ^{1,2} SAM E. CUTLER ¹ RUPALI CHANDAR ³ RICHARD PAN ⁴ DAVID J. SETTON ^{5,*}
LUKAS J. FURTAK ⁶ RACHEL BEZANSON ⁷ IVO LABBE ⁸ JOEL LEJA ^{9,10,11} KATHERINE A. SUESS ¹²
BINGJIE WANG (王冰洁) ^{9,10,11} JOHN R. WEAVER ¹ HAKIM ATEK ¹³ GABRIEL B. BRAMMER ^{14,15}
ROBERT FELDMANN ¹⁶ NATASCHA M. FÖRSTER SCHREIBER ¹⁷ KARL GLAZEBROOK ¹⁸ ANNA DE GRAAFF ¹⁹
JENNY E. GREENE ²⁰ GOURAV KHULLAR ²¹ DANILO MARCHESINI ²² MICHAEL V. MASEDA ²³ TIM B. MILLER ²⁴
HOJUN MO ²⁵ LAMIYA A. MOWLA ²⁶ THEMIYA NANAYAKKARA ¹⁸ ERICA J. NELSON ²⁷ SEDONA H. PRICE ²⁸
FRANCESCA RIZZO ²⁹ PIETER VAN DOKKUM ³⁰ CHRISTINA C. WILLIAMS ^{31,32} YANZHE ZHANG ²⁵
YUNCHONG ZHANG ²⁸ AND ADI ZITRIN ⁶

¹Department of Astronomy, University of Massachusetts, Amherst, MA 01003, USA

²Cosmic Dawn Center (DAWN), Denmark

³Ritter Astrophysical Research Center, University of Toledo, Toledo, OH 43606, USA

⁴Department of Physics and Astronomy, Tufts University, 574 Boston Ave., Medford, MA 02155, USA

⁵Department of Astrophysical Sciences, Princeton University, 4 Ivy Lane, Princeton, NJ 08544, USA

⁶Department of Physics, Ben-Gurion University of the Negev, P.O. Box 653, Be'er-Sheva 84105, Israel

⁷Department of Physics & Astronomy and PITT PACC, University of Pittsburgh, Pittsburgh, PA 15260, USA

⁸Centre for Astrophysics and Supercomputing, Swinburne University of Technology, Melbourne, VIC 3122, Australia

⁹Department of Astronomy & Astrophysics, The Pennsylvania State University, University Park, PA 16802, USA

¹⁰Institute for Computational & Data Sciences, The Pennsylvania State University, University Park, PA 16802, USA

¹¹Institute for Gravitation and the Cosmos, The Pennsylvania State University, University Park, PA 16802, USA

¹²Department for Astrophysical & Planetary Science, University of Colorado, Boulder, CO 80309, USA

¹³Institut d'Astrophysique de Paris, CNRS, Sorbonne Université, 98bis Boulevard Arago, 75014, Paris, France

¹⁴Cosmic Dawn Center (DAWN), Copenhagen, Denmark

¹⁵Niels Bohr Institute, University of Copenhagen, Jagtvej 128, Copenhagen, Denmark

¹⁶Department of Astrophysics, Universität Zürich, Winterthurerstrasse 190, CH-8044 Zurich, Switzerland

¹⁷Max-Planck-Institut für extraterrestrische Physik, Giessenbachstrasse 1, 85748 Garching, Germany

¹⁸Centre for Astrophysics and Supercomputing, Swinburne University of Technology, PO Box 218, Hawthorn, VIC 3122, Australia

¹⁹Max-Planck-Institut für Astronomie, Königstuhl 17, D-69117, Heidelberg, Germany

²⁰Department of Astrophysical Sciences, Princeton University, Princeton, NJ 08544, USA

²¹Department of Astronomy, University of Washington, Physics-Astronomy Building, Box 351580, Seattle, WA 98195-1700, USA

²²Department of Physics & Astronomy, Tufts University, MA 02155, USA

²³Department of Astronomy, University of Wisconsin-Madison, 475 N. Charter St., Madison, WI 53706, USA

²⁴Center for Interdisciplinary Exploration and Research in Astrophysics (CIERA), Northwestern University, 1800 Sherman Ave, Evanston, IL 60201, USA

²⁵Department of Astronomy, University of Massachusetts, Amherst, MA, 01003-9305, USA

²⁶Whitin Observatory, Department of Physics and Astronomy, Wellesley College, 106 Central Street, Wellesley, MA 02481, USA

²⁷Department for Astrophysical and Planetary Science, University of Colorado, Boulder, CO 80309, USA

²⁸Department of Physics and Astronomy and PITT PACC, University of Pittsburgh, Pittsburgh, PA 15260, USA

²⁹Kapteyn Astronomical Institute, University of Groningen, Landleven 12, 9747 AD, Groningen, The Netherlands

³⁰Astronomy Department, Yale University, 52 Hillhouse Ave, New Haven, CT 06511, USA

³¹NSF National Optical-Infrared Astronomy Research Laboratory, 950 North Cherry Avenue, Tucson, AZ 85719, USA

³²Steward Observatory, University of Arizona, 933 North Cherry Avenue, Tucson, AZ 85721, USA

ABSTRACT

Globular clusters (GCs) are some of the oldest bound structures in the Universe, holding clues to the earliest epochs of star formation and galaxy assembly. However, accurate age measurements of ancient clusters are challenging due to the age-metallicity degeneracy. Here, we report the discovery of 42 compact stellar systems

within the ‘Relic’, a massive, quiescent galaxy at $z = 2.53$. The Relic resides in an overdensity behind the Abell 2744 cluster, with a prominent tidal tail extending towards two low-mass companions. Using deep data from the UNCOVER/MegaScience JWST Surveys, we find that clusters formed in age intervals ranging from 8 Myr up to ~ 2 Gyr, suggesting a rich formation history starting at $z \sim 10$. While the cluster-based star formation history is broadly consistent with the high past star formation rates derived from the diffuse host galaxy light, one potential discrepancy is a tentative $\sim 2-3\times$ higher rate in the cluster population for the past Gyr. Taken together with the spatial distribution and low inferred metallicities of these young-to-intermediate age clusters, we may be seeing direct evidence for the accretion of star clusters in addition to their early in-situ formation. The cluster masses are high, $\sim 10^6 - 10^7 M_{\odot}$, which may explain why we are able to detect them around this likely post-merger galaxy. Overall, the Relic clusters are consistent with being precursors of the most massive present-day GCs. This unique laboratory enables the first connection between long-lived, high-redshift clusters and local stellar populations, offering insights into the early stages of GC evolution and the broader processes of galaxy assembly.

Keywords: Globular star clusters(656); Galaxy formation (595); Galaxy evolution (594); Galaxy quenching (2040); James Webb Space Telescope (2291)

1. INTRODUCTION

A hallmark of the standard Λ CDM cosmological framework asserts that galaxies assemble piecewise, continually fueling new generations of star formation via in-flowing gas and the accretion of smaller satellite galaxies. Understanding this process is key to understanding how modern massive galaxies, including our own Milky Way, form and evolve. Direct observations of compact star clusters at high redshift, when the Universe is only a few billion years old, therefore provide critical evidence necessary to map out the hierarchical growth process at the earliest times. This is because ultimately most star formation occurs in clusters (Lada & Lada 2003; Krumholz et al. 2019), with a significant fraction therein occurring in the compact, star-forming clusters observed at early epochs (e.g., Adamo et al. 2020). Therefore, the problem of understanding the structural evolution of galaxies in a hierarchical framework is inherently linked to the density and resulting lifetimes of their building blocks, stellar associations.

Little is known about how and when long-lived, dense globular clusters (GCs) in the Milky Way and nearby galaxies formed. The theoretical consensus is that GCs generally emerge from regions within the interstellar medium with violent conditions, including high gas densities, turbulent velocities, and hence extreme gas pressures (see e.g., Kruijssen 2014). There are thought to be two main GC formation channels, including in-situ formation or the stripping of accreted satellites (Brodie & Strader 2006; Pota et al. 2013; Li & Gnedin 2014; Harris et al. 2015; Forbes & Remus 2018; Dolfi et al. 2021; Kluge et al. 2023). Observationally, both massive elliptical galaxies and spiral galaxies with prominent bulges

have long been known to host two populations of GCs, one that is metal-rich and red, and another that is metal-poor and relatively bluer in color (e.g. Peng et al. 2004; Faifer et al. 2011; Brodie et al. 2012; Usher et al. 2012; Pota et al. 2013).

The origin of the bimodality in GC colors and metallicities remains the most outstanding question of GC formation. The metal-rich GCs have been suggested to have formed either in galaxy mergers (Ashman & Zepf 1992; Beasley et al. 2002; Newton et al. 2024; De Lucia et al. 2024) or coevally with the bulk of the stellar populations within the host galaxy (Forbes et al. 1997; Strader et al. 2005; Chen et al. 2024; De Lucia et al. 2024). Those metal-rich clusters that reside in the halo in particular may have initially formed in proto-disks but are thrown out by merger-driven violent relaxation (Hopkins et al. 2009). On the other hand, the metal-poor GCs may have formed during the collapse of proto-galactic clouds (Forbes et al. 1997; Beasley et al. 2002), which is suggested to have been truncated by reionization (Strader et al. 2005). Another explanation for the bimodality of the GC population is that it is a natural result of hierarchical galaxy formation, in which the metal-poor GCs originate in cannibalized dwarf galaxies (e.g., Côté et al. 1998; Hilker et al. 1999; Kissler-Patig 2000; Mackey & Gilmore 2004). Although the common interpretation is that red, metal-rich GCs predominantly form during the in-situ phase and blue, metal-poor GCs during an accretion phase of massive galaxy formation (e.g., Peng et al. 2004; Pota et al. 2013; Kluge et al. 2023), there is not a strict one-to-one connection (Forbes & Remus 2018). That said, there may be no need for separate formation processes at all, as cluster disruption may explain the bimodal GC metallicity distribution (Pfeffer et al. 2023). While debate continues on the where and the how of GC formation, the age distribution of GCs in galaxies at $z > 1$ can directly address these ques-

* Brinson Prize Fellow

tions given that massive star clusters trace major star-forming episodes in their parent galaxies.

With the first Webb Deep field, SMACS0723, the James Webb Space Telescope (JWST; Gardner et al. 2023) imaging and slitless spectroscopy immediately revealed GC candidates in a strongly-lensed, $z = 1.378$ galaxy (“The Sparkler”, Mowla et al. 2022; Claeysens et al. 2023). Spectrophotometric fitting suggests that these compact, red sources are likely ancient GCs that formed between $7 < z < 11$. For context, GCs in the Milky Way have ages ranging from ~ 11 -13 Gyrs, implying that the oldest Milky Way globular clusters formed at $z \sim 8 - 10$ (Beaulieu et al. 2001; Momany et al. 2003; De Angeli et al. 2005; Marín-Franch et al. 2009; Leaman et al. 2013; de la Fuente Marcos et al. 2015). However, further analysis of the GC candidates in the Sparkler confirm that while most were likely formed very early in the Universe, there is a significant spread in metallicity that calls into question their assembly history (Adamo et al. 2023). The degeneracy between age and metallicity has long stifled our ability to age-date GCs older than a few billion years, resulting in age uncertainties up to 3 Gyr (e.g., De Angeli et al. 2005; Marín-Franch et al. 2009).

The complexity in robustly constraining the ages of both GCs in our Milky Way and nearby galaxies, as well as those in the Sparkler, lies in the fact that they are many billions of years old. Measuring ages for populations > 2 Gyr old is incredibly challenging and observationally expensive owing to their subtly varying colors and spectral features (e.g., Kriek et al. 2009, 2016). Thus, it is difficult to definitively conclude if the ages of GCs approach the age of the Universe, even at $z \sim 1.5$ ($t_{\text{univ}} = 4.5$ Gyr). This technical limitation is inherent to the problem, with only marginal returns even in the case of acquiring high quality, deep spectroscopy. With the first few drips of data from JWST, the Sparkler rapidly became the best known example in the literature to date of a galaxy containing GC candidates at $z > 1$ – the infrared sensitivity of this facility immediately opened a brand new discovery space in understanding GC formation. With the discovery of similarly exciting targets, but at higher redshifts, the age constraints become more meaningful (e.g., see improvements in age constraints for early quenched galaxies; Carnall et al. 2023; Glazebrook et al. 2024; de Graaff et al. 2024).

There is a growing literature of JWST studies of the stellar populations of high redshift clumps, where age-dating is more straight forward owing simply to the young age of the universe itself (Claeysens et al. 2023; Messa et al. 2024a,b; Fujimoto et al. 2024; Welch et al. 2023; Vanzella et al. 2022a, 2023; Bergamini et al. 2023). Possible GC candidates may even now be identified as early as $z = 8 - 10$ (Adamo et al. 2024; Bradley et al. 2024; Mowla et al. 2024). Note that some published works on cluster systems at high redshift use the term ‘clump’ to refer to a wide range of stellar systems,

extending from the most compact sources that could still have sizes of a few 100 pc up to much larger (\approx kpc-scale) super-complexes that are spatially resolved (e.g., Förster Schreiber et al. 2011; Guo et al. 2015, 2018). However, measurements in highly lensed systems can provide improved constraints for the sizes of stellar sources, reaching half-light radii of just a few pc (and even measured sizes in a handful of cases; Vanzella et al. 2022b, 2023); we therefore will refer to the compact (unresolved) stellar sources which have estimated ages of at least 10 Myr as ‘clusters’ or ‘globular clusters’, since they have likely survived early dispersal and can be considered gravitationally bound.

Hunting for the oldest bonafide GC candidates that have well passed this threshold to survive disruption limits the redshift range effectively to $z < 5$, whereas complexities in constraining age bookend this limit to $z \gtrsim 2$ (i.e., $1 < t_{\text{univ}} < 3$ Gyr). Studies in this redshift space have discovered many star clusters, but all are limited to ages < 300 Myr (Vanzella et al. 2022b; Messa et al. 2024a). Moreover, the host galaxies all appear to be actively star-forming, similar to the rich history of earlier Hubble Space Telescope giant clump studies (e.g., Förster Schreiber et al. 2011; Wuyts et al. 2012; Guo et al. 2012, 2015, 2018). A recent comprehensive analysis of star clusters within galaxies behind the Abell 2744 cluster expands this parameter space (Claeysens et al. 2024), though only 3 out of 1956 clusters fall in the relevant age (> 800 Myr) and redshift range ($z > 2.5$) that would correspond to first GC candidates unambiguously capable of surviving to the present day.

In this work, we report the discovery of a remarkable laboratory: a quenched, $\log(M_*/M_\odot) = 10.86_{-0.16}^{+0.04}$ galaxy¹ (A2744-DR2-35602) at $z_{\text{phot}} = 2.53_{-0.36}^{+0.12}$ with an extended smooth light profile, scattered with compact stellar systems that may be the earliest known GCs (Figure 2). A2744-DR2-35602, hereafter “The Relic,” is a classical quiescent galaxy first identified in the Cycle 1 JWST UNCOVER Treasury Program (JWST-GO-2561; PIs: Labbé/Bezanson, Bezanson et al. 2024) photometric catalog (Weaver et al. 2024). The Relic is a remarkably bright ($F444W = 20.52$ ABmag) quiescent target ($\log(\text{sSFR}/\text{yr}^{-1}) = -9.61_{-0.15}^{+0.51}$, i.e., ~ 1 dex below the main-sequence from Speagle et al. (2014); Leja et al. (2022)). The Relic features a large, extended de Vaucouleurs-like light profile, with a tidal tail connecting it to two lower mass quiescent galaxies consistent with the same redshift. The system of galaxies reside in the northwest outskirts of the strong lensing cluster Abell 2744, outside of the caustic. As such, the Relic and its two neighbors have modest magnifications of $\mu \sim 2.7$ (Furtak et al. 2023), with ultra-deep imaging in the complete suite of medium-band and broad-

¹ This value is corrected for magnification.

band JWST/NIRCam filters from 0.7-4.4 μ m when also including Cycle 2 data from JWST-GO-4111 (PI: Suess; [Suess et al. 2024](#)). While ultra-deep follow-up IFU spectroscopy of the Relic was acquired on October 28, 2024 and December 15-16, 2024 through a Cycle 3 program (JWST-GO-6405, PIs: Cutler, Whitaker), we focus herein on the photometric properties of this target over a significantly wider field of view relative to the two 3'' IFU footprints. The purpose of this paper is to report the physical properties of the GC candidates derived from the JWST imaging dataset, whereas spectroscopic redshift confirmation and a more detailed resolved spectral analysis will come with the Cycle 3 data. The paper is organized as follows: Section 2 presents the data reduction, details on the source detection, photometry, and photometric redshift and spectral synthesis modeling is found in Section 3, the resulting stellar population trends are summarized in Section 4, and we place our findings in the context of our current understanding of GC formation in Section 5.

We assume a [Chabrier \(2003\)](#) initial mass function (IMF) and a standard concordance cosmology: $H_0 = 70 \text{ km s}^{-1} \text{ Mpc}^{-1}$, $\Omega_M = 0.3$, and $\Omega_\Lambda = 0.7$. All magnitudes in this paper are expressed in the AB system ([Oke 1974](#)), for which a flux f_ν in $10 \times \text{nJy}$ ($10^{-28} \text{ erg cm}^{-2} \text{ s}^{-1} \text{ Hz}^{-1}$) corresponds to $\text{AB}_\nu = 28.9 - 2.5 \log_{10}(f_\nu / \mu\text{Jy})$.

2. DATA

The Relic ($\alpha, \delta = 3.5277082, -30.3665864$) was first identified in the extended coverage afforded by the UNCOVER treasury program (JWST-GO-2561; PIs: Labbé, Bezanson [Bezanson et al. 2024](#)), including 45 sq. arcmin of near-infrared imaging of the strong gravitational lensing cluster Abell 2744. The original UNCOVER NIRCam image set includes F090W, F115W, F150W, F200W, F277W, F356W, F410M, and F444W, later augmented by 12 additional bands (F070W, F140M, F162M, F182M, F210M, F250M, F300M, F335M, F360M, F430M, F460M, and F480M) through the Cycle 2 MegaScience Program (JWST-GO-4111, PI: Suess; [Suess et al. 2024](#)) and additional integration in F070W and F090W filters through the Cycle 2 ALT Program (JWST-GO-3516, PIs: Matthee, Naidu; [Naidu et al. 2024](#)). The combined data set is one of the deepest-to-date (when augmented by strong lensing) publicly available Webb surveys ([Bezanson et al. 2024](#); [Suess et al. 2024](#)).

The data presented in this paper were originally obtained from the Mikulski Archive for Space Telescopes (MAST) at the Space Telescope Science Institute. All images correspond to the v7² mosaics reduced by GRIZLI ([Brammer 2023](#)) and rescaled to a 40 mas pixel scale in all available filters. The observations can all be accessed at <https://doi.org/10.17909/nftp-e621>, with the original photometric catalogs available

at <https://doi.org/10.5281/zenodo.8199802>. While the UNCOVER mosaics formally have bright cluster galaxies, intracluster light, and sky background removed, as described in [Weaver et al. \(2024\)](#), the Relic is sufficiently far from the cluster core that these effects are not important. We do however note two moderately bright sources within an arcsecond of the main target and describe how we remove their contaminating light in Section 3.

We adopt an updated version of the strong lens model from [Furtak et al. \(2023\)](#). The Relic is located in a moderate-magnification region with an average magnification factor of $\mu = 2.75^{+0.12}_{-0.28}$ (with $\mu_{\text{radial}} = 1.10^{+0.01}_{-0.02}$ and $\mu_{\text{tangential}} = 2.49^{+0.09}_{-0.12}$). All photometric measurements have been corrected for this flux boost, assuming the average magnification value. While the statistical uncertainty remains small in this low-magnification regime, systematic modeling uncertainties are expected to be on the order of 20% ([Zitrin et al. 2015](#); [Atek et al. 2024](#)). These uncertainties have been incorporated into the photometry.

We adopt a redshift of $z = 2.53$ herein for the Relic and all associated cluster modeling. With the 20-band photometry, the redshift probability distribution for the Relic returns three viable solutions: (1) $z = 2.28$, (2) $z = 2.53$ (our fiducial value), and (3) $z = 2.68$. The $z = 2.53$ solution is favored when fitting the photometry using Prospector- β ([Wang et al. 2023, 2024](#)), whereas EaZY favors the $z = 2.28$ solution. Medium resolution ($R \sim 1600$) grism spectroscopy in the range of $\sim 3\text{-}4\mu\text{m}$ is publicly available for the Relic (JWST-GO-3516; PIs: Matthee, Naidu; [Naidu et al. 2024](#)); however, only one roll angle is usable and the spectrum extracted for the Relic is noisy. From this spectrum, we confirm that no emission lines are present, supporting the quiescent nature of the Relic. We also find tentative evidence for a broad Pa γ ($\lambda_{\text{rest}} = 1.094\mu\text{m}$) absorption feature consistent with a spectroscopic redshift of $z = 2.524$. However, we note that if Pa γ were observable, we also should have seen Pa δ , which was not detected. While a proper reduction of the recent deep IFU data is not completed, we see tentative evidence for a break consistent with $z = 2.53$. Finally, in contrast, there does appear to be one cluster (ID8) that may have emission-line boosting that is only possible with the $z = 2.68$ solution; while this cluster may not be physically associated with the Relic, the solution of $z = 2.53$ is within the posterior distribution function.

Other evidence supporting the $z = 2.5$ solution includes the discovery of a large overdensity of ~ 100 quiescent galaxies at $z = 2.5$ within the Abell 2744 field of view ([Naidu et al. 2024](#), ; see also [Pan et al. 2025](#), in prep). There exists a faint extended tidal tail to the south of the Relic, connecting the main target with two lower-mass ($\log(M/M_\odot) \sim 9$) quiescent galaxies about 70 kpc away (~ 30 kpc in the source plane). Figure 1 shows the spectral energy distributions and best-fit models for these sources adopting the Prospector- β physical

² <https://dawn-cph.github.io/dja/imaging/v7/>

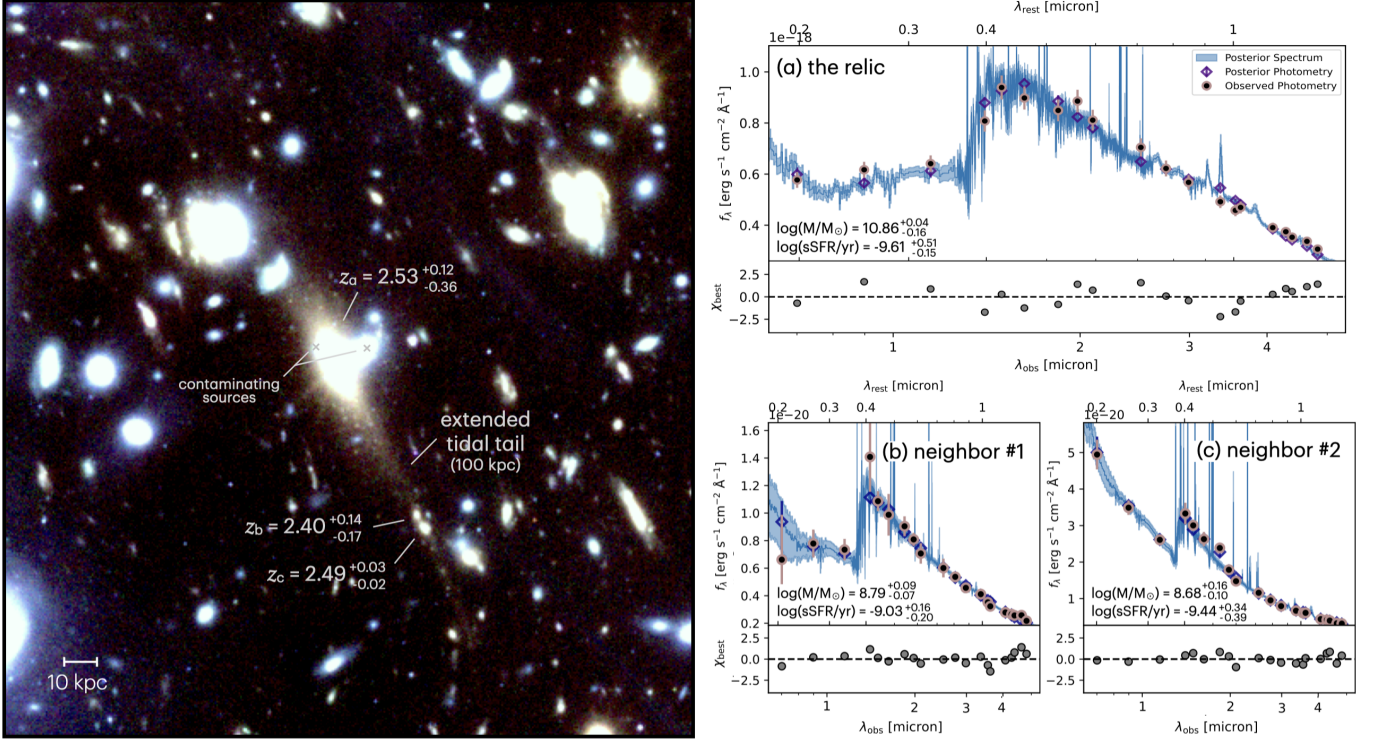


Figure 1. **Left:** Composite color image (F277W, F356W, and F444W) of the Relic (a) and two lower mass neighboring galaxies to the bottom right (b and c) connected by a diffuse tidal tail that extends roughly 100 kpc (40 kpc in the source plane). **Right:** The spectral energy distributions of the three galaxies are all consistent with being quiescent. The photometric redshifts for all three are consistent within the uncertainties. The scale bar is in the observed plane, whereas the source plane scale is roughly the same perpendicular to the main axis of the Relic and a factor of 2.5 smaller parallel to the main axis.

model with a non-parametric star formation history (Wang et al. 2024). Their photometric redshifts, $z_{\text{phot,b}} = 2.40^{+0.14}_{-0.17}$ and $z_{\text{phot,c}} = 2.49^{+0.03}_{-0.02}$, are consistent with the Relic having recently passed by, with a tidal stream marking the past trajectory. All together, while we find ample evidence to support the $z = 2.53$ solution as our fiducial value (and a spectroscopic redshift will be coming soon), we are careful to test the impact of alternative redshift solutions on our conclusions for all subsequent analyses.

3. METHODS

3.1. Cluster Detection

Figure 2 shows the composite color image (F277W, F356W, and F444W) of the Relic before (left) and after (right) subtracting the smooth elliptical light profile of the host galaxy. Sources are detected by running Source Extractor (Bertin & Arnouts 1996) on a detection image, which is created by dividing the original images (Figure 2, left) by a median filtered image version in 4 filters (F200W, F277W, F356W, F444W) and combining them together (e.g., Goudfrooij et al. 2001). The smoothing scale is set to 9 pixels, but we note that a range from 7 to 10 pixels is acceptable and identifies the same sources unambiguously. In order to robustly identify clusters in the vicinity of the Relic,

we experiment with first removing two moderately bright nearby galaxies (marked with crosses in Figure 2) before median dividing the smoothed image versus the outcome when not subtracting these neighbors. While the removal of these nearby sources following the methodology detailed in Weaver et al. (2024) (i.e., subtracting smooth elliptical light profiles) leaves residuals at the galaxy core for the brighter of the two, this is a trade off with the benefit of also removing extended light that could contaminate the cluster photometry. We also experiment with running the source detection directly on the galaxy-subtracted image (Figure 2, right), but find that we can more robustly identify compact sources when using the median smoothing technique described above. We retain 44 sources that are detected above a signal-to-noise ratio (SNR) threshold of 3 in F444W and 2 in F200W and proceed to vet this sample through an analysis of their spectral energy distributions (SED), as described in the following sections.

Regardless of the detection approach adopted, no new candidate clusters are discovered close to the bright center of the Relic (see Figure 2). As we consider the region within the central $\lesssim 10$ kpc radius (~ 4 kpc in the source plane along tidal tail axis) to be contaminated by residual features with minimal contrast possible between the host light and candi-

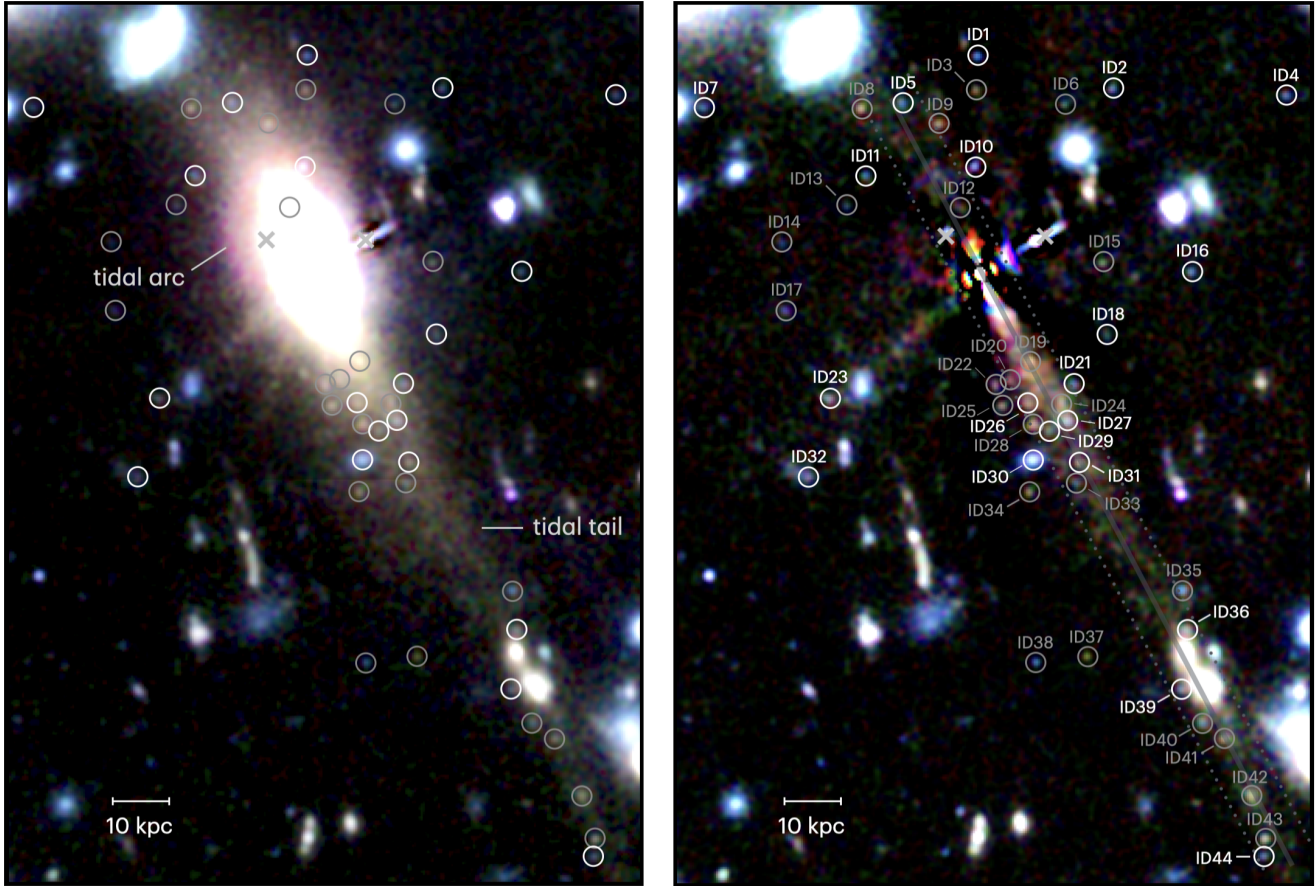


Figure 2. Composite color image (F277W, F356W, and F444W) of the Relic before (left) and after (right) subtracting the main host galaxy. All point sources with a photometric redshift consistent with the main target ($z_{\text{phot}} = 2.53$) and $\text{SNR} > 3$ in F444W are encircled, shown as white if the best-fit simple stellar population has a reduced $\chi^2 < 2$ and grey where reduced $\chi^2 > 2$. The scale bar is in the observed plane, whereas the source plane scale is roughly the same perpendicular to the main axis of the Relic and a factor of 2.5 smaller parallel to the main axis.

date clusters, we can neither confirm nor rule out the absence of clusters within this galactocentric radius.

3.2. Cluster Photometry

Before extracting photometry of the detected point sources, all images are homogenized to a common resolution matching the F444W point spread function (PSF). We use the same convolution kernels as developed and extensively tested in Weaver et al. (2024) and Suess et al. (2024). The kernels are derived from matching empirical PSFs built from stars selected across the UNCOVER footprint using `pypher` (Boucaud et al. 2016). Due to the dither pattern and conditions at the time of observations, the empirical PSFs are broader than those produced by WebbPSF. Thus, the use of an empirical PSF is particularly important when deriving the morphologies and/or colors of compact objects.

Given the complex background light surrounding the GC candidates, we opt to use background-subtracted images for the photometric analysis, with both the neighboring galaxies and smooth light profile of the main Relic subtracted out (Figure 2, right). We perform photometry on these

background-subtracted, psf-convolved images within circular apertures of $0.16''$ diameter owing to the compact nature of the clusters (see Section 3.3 for more details); such a small aperture maximizes the SNR recovered for the extracted photometry of compact sources. In order to correct to total flux, we estimate the aperture correction by measuring the amount of light from F444W UNCOVER empirical PSF curve of growth that falls outside of a radius of $0.08''$. The value of this correction factor is 2.72 for all PSF homogenized filters. All fluxes are corrected for galactic extinction, with a maximum correction of 0.02 ABmag in F070W. Finally, the flux densities are further systematically down-weighted by the magnification factor at the location of the Relic, $\mu = 2.75$. While performing photometric validation checks, we noticed that the short-wavelength (SW) medium-band images had mild residual striping effects in the background. While the variations are mild, such background variations become important when measuring photometry for objects close to the noise level, and even more so for intrinsically red clusters that are fainter in these blue SW filters. We therefore increase the error bars for all SW medium-band flux density measure-

ments (F140M,F162M,F182M,F210M) by 30% and set the flux to a null value if the SNR is less than unity (i.e., flux = NaN). We experimented with different assumptions (i.e., boosting the flux uncertainties higher, removing all medium-band filters, etc), but this did not significantly change the results.

The aperture photometry of the Relic itself was performed following the methodology outlined in [Weaver et al. \(2024\)](#) and adopted from the publicly released “super” photometric catalog. Briefly, aperture photometry is performed on the bCG-subtracted images that are all homogenized to the F444W PSF. In the “super” catalog, the aperture chosen scales with the spatial extent of the object, ranging from 0.32 arcseconds upwards to 1.4 arcseconds in diameter. The aperture diameter adopted for the Relic is 0.48 arcseconds. The flux is then scaled to total through aperture corrections that first scale up all filters by the same amount based on the ratio of the flux within the larger Kron radius relative to the circular aperture, and a second correction to account for missing light outside the Kron radius inferred from the empirical F444W PSF curve of growth analysis. In this approach, the spectral shape and colors of the Relic correspond to the light within the 0.48 arcsecond diameter. The main host galaxy photometry therefore does not overlap spatially with any clusters detected, as they are all located beyond an arcsecond from the center, and can be treated as a distinct photometric analysis.

3.3. Constraints on Cluster Sizes

In order to demonstrate that the cluster candidates are unresolved, we model the light for all sources isolated from the tidal tail in the band with the highest SNR ratio – most often F200W. We perform a single Sersic profile fit on the original image (before PSF homogenization) using `galfit` ([Peng et al. 2010a](#)), adopting the settings described in [Cutler et al. \(2022\)](#). While we did attempt to model all clusters, we find that the fits fail when it is embedded within the diffuse tidal tail light as `galfit` cannot robustly determine the background level. Luckily, the failure mode of `galfit` returns spectacularly large, extended best-fit models that are easy to identify. We find 9 clusters for which the models and residuals appear reasonable. While this morphological analysis therefore only includes 20% of the sample, it is likely the best we can do given the faintness of these clusters candidates and the background contamination.

For the 9 cluster candidates modeled, we find a median effective radius of 0.01 arcseconds with a standard deviation of 1.13 arcseconds (not correcting for magnification); the latter value is completely driven by an asymmetric distribution with two outliers. These effective radii measurements are mostly inferred from the F200W image, but F444W has highest SNR in two cases and F277W in another. We find that the

sample includes two moderately bright, blue sources which show tentative evidence for extended light profiles. ID30 is located moderately close to the tidal tail with an effective radius of 0.36 arcseconds, and ID32 is in the halo but has a visible blue “smudge” attached to it. As both fits are inconsistent with being unresolved, we caution the reader that ID30 and ID32 are likely not cluster members and we remove them from the subsequent analysis on the basis of their size estimates. The median size decreases to 0.007 ± 0.008 arcseconds when excluding ID30 and ID32. A mock recovery test quantifying the limit down to which we can recover sizes performed by [Cloonan et al. \(in prep\)](#) suggests that values below roughly 0.08-0.2 arcseconds (depending on the filter adopted) can be considered unresolved. At the best JWST resolution scales and given the modest magnification at the location of the Relic, these clusters have upper limits as low as roughly 100 pc in the source plane. While this value is significantly larger than the typical half light radius of local GCs of $\sim 1-10$ pc (e.g., [Jordán et al. 2005](#); [Spitler et al. 2006](#)), this motivates the requirement for sources to be unresolved.

3.4. Final Cluster Sample

We detect 44 compact sources within a radius of ~ 7 arcseconds of the Relic that pass our SNR requirements, including additional search area extended along the full extent of the tidal tail. Given the radial and tangential magnifications, this corresponds to a search radius of roughly 50 kpc in the source plane perpendicular to the main axis ($\mu_t = 1.1$) and ~ 40 kpc along the tidal tail axis ($\mu_t = 2.5$). The morphological analysis removes ID30 and ID32 from our final sample, which are formally resolved and thus correspond to larger star-forming complexes. To test for additional interlopers, photometric redshifts of all stellar sources are computed using EAzy ([Brammer et al. 2008](#)), fitting all 20 JWST bands available for each candidate with a linear combination of galaxy templates. Following [Weaver et al. \(2024\)](#), we increase the minimum error floor from the default value of 1% to 5% in order to more realistically reflect the calibration uncertainties of JWST/NIRCam data. We forgo the pre-processing step of iteratively tuning zero-points in order to avoid biasing our colors to those of the SED templates, also turning off both magnitude and β -slope priors for similar reasons. All red sources are consistent with the redshift of the Relic within uncertainties. Specifically, we mentioned earlier that ID8 has possible emission-line boosting that would support a $z = 2.68$ redshift solution; however, we do not remove this cluster from our sample as the $z = 2.53$ solution is still within the redshift posterior. While the bluest sources (see Figure 4) have very low redshift solutions that are formally inconsistent ($z < 0.1$), the EAzy template set cannot accommodate for higher redshift solutions for these particular objects. However, a subsequent analysis demonstrates

that young simple stellar populations at $z = 2.53$ can describe well these spectral shapes, and importantly are expected to exist. We therefore do not identify any additional sources to remove from this analysis, though we do perform a series of tests to further justify the inclusion of the blue sources (see Section 3.5).

Our final sample is comprised of the 42 remaining point sources with sufficient SNR in F200W and F444W, all with redshift probability distribution functions and/or spectral shapes consistent with that of the Relic. The location of these likely clusters are marked in right panel of Figure 2.

3.5. The Origin of the Blue Clusters

We note that the majority of detected clusters, especially those unambiguously in the halo, have relatively blue featureless SED shapes with no obvious emission-line boosting. In principle, these SEDs may also be consistent with foreground cluster candidates either in the Abell 2744 intra-cluster medium or the far outskirts of a bright cluster galaxy. As visible in Figure 2, the nearest bright cluster galaxy is about 20 arcseconds away. Globular clusters associated with this galaxy would reside at a distance of around 160 kpc, not completely unrealistic but at the extremes of GC radial studies (for reference, the most distant GC in the Milky Way is located nearly 150 kpc away; [Laevens et al. \(2014\)](#)).

With featureless spectra and no coverage of the 4000 break or blueward at $z = 0.308$, we cannot rule out the possibility that these blue clusters are unassociated with the Relic. Deep F336W HST imaging reaching 29 ABmag, coming either mid-2025 or mid-2026 (HST-GO-14622; PIs: Whitaker, Bezanson, Leja), will provide coverage either of the rest-UV (in the case of $z = 0.308$) or yield a null detection (below the Lyman limit at $z = 2.53$). However, given their proximity to the Relic, and that they are found symmetrically around the galaxy, it is likely that they are associated with the Relic.

We can further assess if the blue clusters in our sample are associated with the Relic based on space density arguments. We estimate the space density of clusters in the Abell 2744 by adopting a cluster catalog created following an approach similar to [Harris & Reina-Campos \(2023\)](#), selecting all clusters above a magnitude limit ranging from 29 ABmag to 30 ABmag. The area of the Abell 2744 is calculated to be the region where the magnification is greater than 1.5, a conservative estimate of 18.7 arcmin². We perform the same analysis on the Relic clusters that lie within the 7 arcsecond search radius, which corresponds to an area of 0.04 arcmin² in the image plane and 0.016 arcmin² in the source plane. We find the space density of clusters in the Relic is $\sim 6-12\times$ higher, with a value of 0.29 clusters/arcsecond² in the Relic versus 0.03 clusters/arcsecond² in Abell 2744 for clusters brighter than a limit of 29.5 ABmag. Both studies would not be sensitive to detecting clusters close to the host galaxy, so this is

likely a fair comparison. If we only consider the blue clusters in this analysis (assuming the red clusters are unambiguously associated with the Relic), restricting to $V-I < 0$, this overdensity decreases to a factor of $5-9\times$ higher. In either case, the space density of clusters surrounding the Relic is $> 5\times$ higher relative to the Abell 2744 clusters. Moreover, the radial distribution of the clusters surrounding the Relic is also roughly similar in number to that of the Milky Way for distances of 5–10 kpc and greater ([Harris 1996](#)). We thus conclude that these clusters are likely associated with the Relic.

3.6. Stellar Population Synthesis Modeling

We model the photometry of the clusters using the `prospector` Bayesian inference framework ([Johnson et al. 2021](#)), adopting the MIST stellar isochrones ([Choi et al. 2016](#); [Dotter 2016](#)) and MILES stellar library ([Sánchez-Blázquez et al. 2006](#)) from the Flexible Stellar Population Synthesis (FSPS) stellar population synthesis models ([Conroy et al. 2009](#)). Our fiducial model for all stellar sources is a simple single burst star formation history (SFH), which is generally representative of GC formation. For all models, we adopt a [Chabrier \(2003\)](#) IMF and the [Kriek & Conroy \(2013\)](#) two-component dust law. The stellar metallicity has a top-hat prior ranging from a $\log(Z/Z_{\odot})$ value of -2 to 0.2. We also fit within the model for nebular emission (both line and continuum). The models consists of 7 free parameters (M_{*} , age, dust2, $\log Z$, dust_ratio, dust_index, and gas_logU), with sampling performed using the dynamic nested sampler `dynesty` ([Speagle 2020](#)). We fix the redshift to $z = 2.53$ for all sources.

Motivated by empirical results demonstrating that star clusters do not experience significant dust attenuation beyond 10 Myr (e.g., [Whitmore et al. 2020](#); [Chandar et al. 2023](#)), we add an additional age-dust prior to the simple stellar population modeling. We adopt a truncated normal distribution where the total dust extinction A_V exponentially drops from $A_V = 4$ for an age of 1 Myr to 0.1 by 10 Myr, with an upper bound of $A_V = 8$, a lower bound of zero, and a sigma of 3. By 10 Myr, the ionizing photon production is almost gone and feedback has essentially removed the interstellar medium ([Charlot & Fall 2000](#)). The allowable range of values scales down to $A_V=0-0.1$ mag by 10 Myr and beyond. We tested several permutations of this dust prior, but found the results were not significantly impacted. This age-dust prior is not used for any non-parametric SFH modeling cases tested herein, where it is no longer an appropriate assumption.

While we subtract the light from the Relic, the cluster light may still have to travel through some of this diffuse host galaxy light and may therefore be affected by dust obscuration. The most robust way to address this concern is through a joint spectrophotometric analysis of the host and cluster

light using the IFU spectroscopy. However, in order to test the impact of our dust assumptions on the resulting stellar masses and ages based on photometry alone, we re-run all fits instead allowing dust to be free. We find that the clusters are on average 0.04 dex more massive, 300 Myr younger, with an average A_V of 0.4 mag. However, the fits still return solutions for old clusters and the overall trends remain the same. Given that our subsequent interpretation of the formation history of the Relic does not significantly change when allowing dust to be free in the modeling analysis, we defer a more comprehensive dust analysis to future work that includes the IFU spectroscopy.

We split the results of our modeling analysis into two groups based on goodness of fit. We find 22 clusters with a reduced $\chi^2 < 2$ (including ID30 and ID32, which did not make it into the final sample based on morphology), all indicated with white circles in Figure 2, and 22 clusters have reduced $\chi^2 > 2$ (grey circles). We summarize the results of our stellar population modeling in the following section.

4. RESULTS

Figure 3 shows the observed color-color diagram for the Relic clusters in filters roughly equivalent to the rest-frame B-V (F150W-F200W) and V-I (F200W-F277W) at $z = 2.5$. While in principle the added coverage of the medium-band filters is useful, these images are not as deep and the SW filters have noticeable residual background effects. For this reason, we only show a color-color diagram using the deeper broadband filters. Comparing these broadband colors via aperture photometry to both the model tracks from Bruzual & Charlot (2003) and our inferred (color-coded) stellar association ages is a logical sanity check of our more complex modeling efforts and assumptions. The thick model line represents a lower metallicity, at 25% of the Solar value, whereas the thin line is for models with Solar metallicity. We find three broad groups of clumps in color space: those with blue colors and ages predominantly in the range of 8-20 Myr, an intermediate group with ages ranging from 100-600 Myr, and an older population with ages >1 Gyr, close to the mass-weighted age of the Relic itself (star symbol) and the diffuse light of the tidal tail (square symbol). Among the clumps younger than 10 Myr, the typical dust attenuation is 0.2 mag, with a preferred low dust index value of -0.9 (see arrow in Figure 3). As is often the case, the intrinsically red clumps are faint and thus carry the largest uncertainties. The three outliers with red V-I and blue B-V colors (ID31, ID40, and ID43) are located within a few kpc of the tidal tail with SEDs that show clear breaks marked mostly by upper limits in the rest-UV and a highly uncertain B-band magnitude that contributes to the atypical colors on this diagram. These uncertainties aside, we find that the best-fit ages and observed colors are broadly consistent.

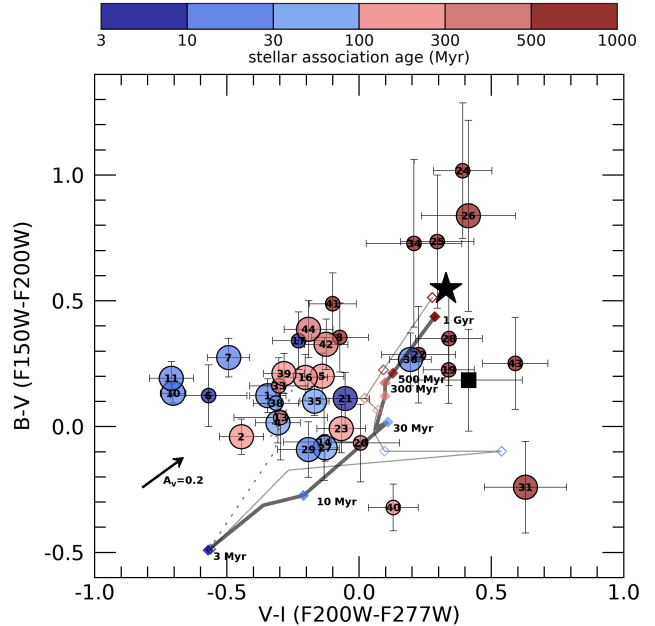


Figure 3. Pseudo B-V versus V-I rest-frame color-color diagram through the F150W, F200W, and F277W filters for all compact sources detected near the Relic and the two neighboring galaxies along the tidal tail (see Figure 1). The symbols are color-coded by the age of their best-fit simple stellar population model, where larger symbols represent fits with reduced $\chi^2 < 2$ and smaller circles are for reduced $\chi^2 > 2$. The color of the main Relic is indicated with a star and diffuse light in the tidal tail with a square symbol. The arrow represents the typical dust attenuation for ages less than 10 Myr of 0.2 mag, assuming the median dust index value of -0.9. FSPS model tracks for 25% Solar metallicity at $z = 2.53$ are shown (solid line), with Solar metallicity indicated with a thinner higher transparency line. The 25% Solar metallicity FSPS model track for the same three filters but now at $z = 0.308$, the redshift of the Abell 2744 cluster, is shown with a dotted line.

The SEDs for the 22 clusters with best-fit model statistics of reduced $\chi^2 < 2$ are shown in Figure 4. Note that we show the SEDs of ID30 and ID32 for comparison, with the IDs marked with asterisks and the clusters crossed off in the central panel of Figure 4, but these sources have been removed on the premise of their spatially resolved sizes. ID30 and ID32 are not included in any subsequent science plots or analyses. The blue shaded region in each SED shows the 16th, 50th and 84th percentile ranges. The maximum a posteriori (MAP) spectrum for the youngest clusters is often outside of the full 16th-84th distribution. Further inspection of the age distributions reveals asymmetry, with a roughly one-sided Gaussian peaked at ages of 8-10 Myr. For all of these cases we adopt the best-fit MAP age as our fiducial and adjust the upper limit to be the 50th percentile.

The middle false color image in Figure 4 shows the full sample of 44 stellar sources, of which 42 comprise our final sample, with the color of each circle represented by the age

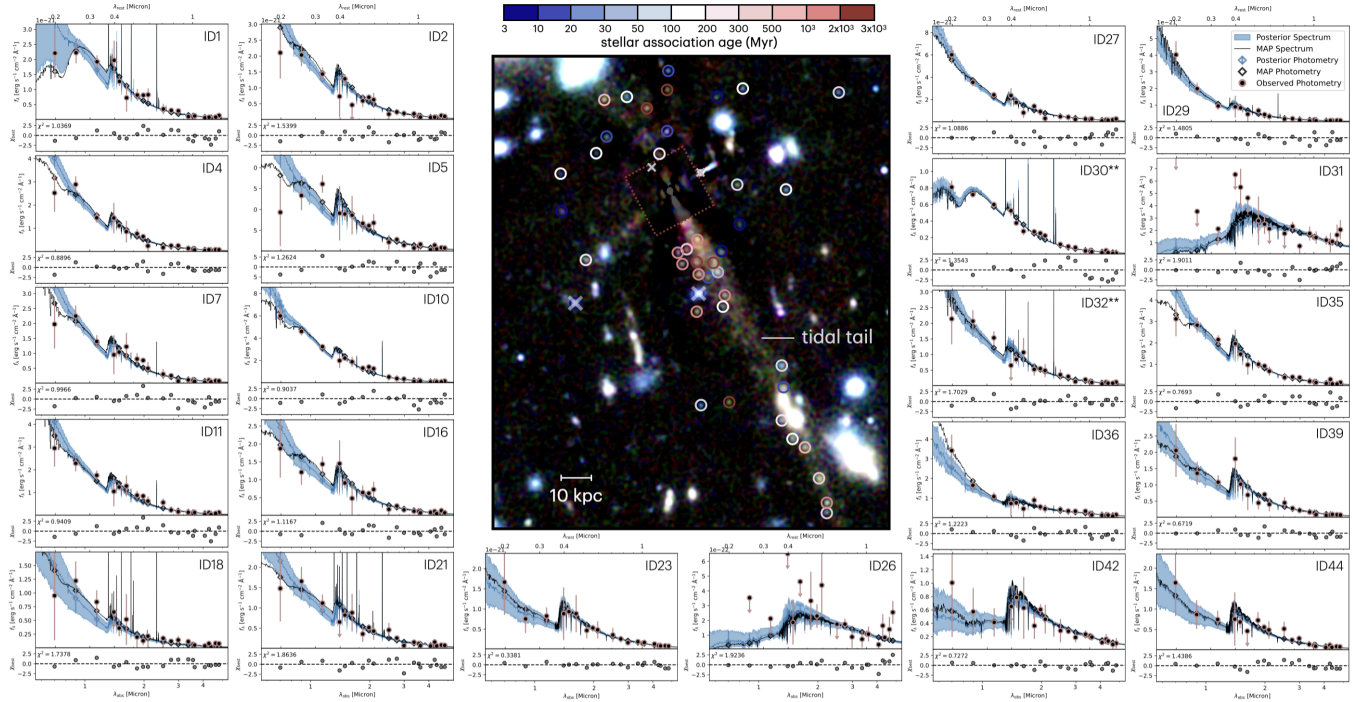


Figure 4. Example spectral energy distributions of the 22 stellar clusters with reduced χ^2 of the best-fit simple stellar population less than 2 at $z = 2.53$. The middle color image shows all 44 detected sources, with the apertures color-coded by the maximum a posteriori (MAP) spectrum from the single burst modeling analysis. Note that ID30 and ID32 are removed from the science analysis. The scale bar is in the observed plane, whereas the source plane scale is roughly the same perpendicular to the main axis of the Relic and a factor of 2 smaller parallel to the main axis.

of the MAP solutions. In general, clusters unambiguously in the halo have younger ages in the range of 9–200 Myr, and those embedded within the tidal tail are generally older with ages ranging from 200 Myr upwards to > 1 Gyr. The oldest clusters are both within the tidal tail and closest to the Relic at radial distances of 10 to 20 kpc. This can also be seen more explicitly in Figure 5, as described next.

We next consider the physical properties of the clusters in Figure 5. We see a clear trend where older clusters have systematically larger stellar masses, although the data are not sensitive to faded, lower mass older clusters. Each symbol is color-coded by the projected scale height above the tidal tail axis. The majority of older clusters lie within a few kpc scale height of the tidal tail main axis, engulfed within the diffuse light, with many close to the main galaxy (not in the halo). The estimated age of the Relic itself is shown as a vertical line. The solid line represents the mass-weighted age of $1.65^{+0.40}_{-0.18}$ Gyr when modeling the photometry released in [Suess et al. \(2024\)](#) (Figure 1) with a non-parametric SFH (Figure 6) that adopts a mass-metallicity prior from [Gallazzi et al. \(2005\)](#). We also fit the same photometry with a single burst SFH (dashed line in Figure 5), but note that this fit cannot adequately describe the full SED shape, either finding a younger post-starburst age that over-predicts the strength of the Balmer-break (the solution shown in Figure 5), or an older age consistent with the non-parametric SFH best-fit that

cannot describe the rest-UV light well. In either case, the Relic is consistent overall with a moderately old stellar population, older than the majority of the associated clusters.

From the top axis of Figure 5, we see the formation redshift inferred for each cluster. This ranges from the epoch of observation at $z = 2.5$ for the youngest clusters up to $z > 10$ for the oldest clusters. The majority of clusters were formed at $z = 2.7$ or earlier. Note that the age of the universe at $z = 2.53$ is only 2.5 Gyr, or a lookback time of almost 11 Gyr. The ages of nearby GCs range between roughly 11 and 13 Gyr (e.g., [De Angeli et al. 2005](#); [Marín-Franch et al. 2009](#); [Ying et al. 2023, 2024](#)). While these dense star clusters are often thought of as some of the oldest structures in the universe, their formation redshifts likely includes $z = 2.5$ (where we observe the Relic) and earlier.

5. DISCUSSION

5.1. Cluster Population in the Relic

The discovery of the Relic at $z = 2.53$ presents a unique opportunity to establish the first direct connection between the formation of long-lived, stellar clusters at high redshift and local stellar populations. At the peak epoch of star formation, this massive quiescent galaxy exists at a time that bookends the era of globular cluster formation, with cluster ages ranging from less than 10 Myr up to 2 Gyr. If we were to fast-forward these stellar associations to the present day,

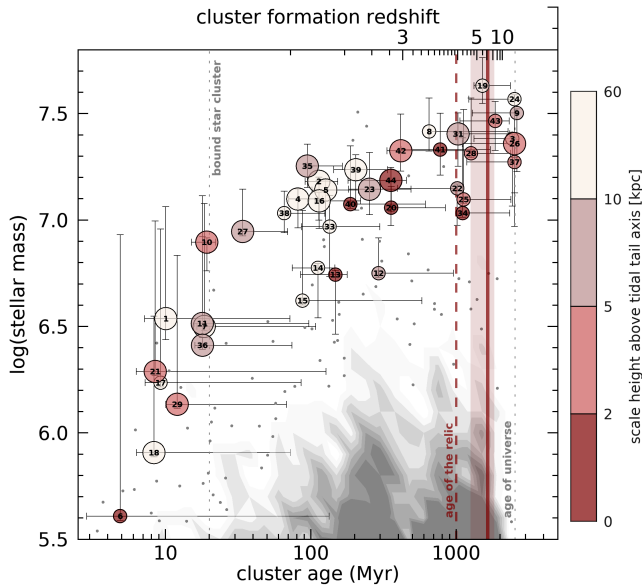


Figure 5. Clusters near the Relic are generally more massive and older. The color-coding represents the scale height above the tidal tail axis (which is close to the source plane value given $\mu_t = 1.10$), with the tidal tail extending roughly 100 kpc from the center of the Relic (or 40 kpc in the source plane, with $\mu_t = 2.49$). The average ages of the Relic (vertical maroon lines) when adopting either a non-parametric SFH (solid line) or a simple stellar population (dashed line) are shown for reference. The top axis shows the cluster formation redshifts relative to the age of the Universe at $z = 2.53$ (dotted line). The Relic clusters are consistent with the extremes of model predictions at $z = 2.5$ from Pfeffer et al. (2024) (greyscale contour and individual grey points for outliers; see Section 5.3 for more details).

their ages would range from 11 to 13 billion years, should they survive disruption (more below).

The clusters have estimated masses of $\approx 10^6 M_\odot$ up to $\approx \text{few} \times 10^7 M_\odot$. This overlaps with local samples of interacting and post-merger galaxies which have formed clusters with similar ages and with similarly high masses, of order 10^7 - $10^8 M_\odot$, including the Antennae (He et al. 2022), NGC 34 (Schweizer & Seitzer 2007), and NGC 7252 (Schweizer & Seitzer 1998). Note however, that clumps discovered in other more highly magnified systems have estimated half-light radii ranging from ≈ 20 pc down to 1 pc (e.g., the Sunburst arc at $z=2.37$ and Sunrise Arc at $z\sim 6$; Vanzella et al. 2022b, 2023). These smaller sizes are very similar to those measured for GCs in nearby elliptical and spiral galaxies including the Milky Way (e.g., < 1 pc to 8 pc; Kundu & Whitmore 1998; Kundu et al. 1999; Larsen et al. 2001; Jordán et al. 2005; Spitler et al. 2006). Taken together, the Relic presents a compelling case where we are observing bonafide GCs soon after they formed, as evidenced by their derived ages, stellar masses, and (unresolved) sizes.

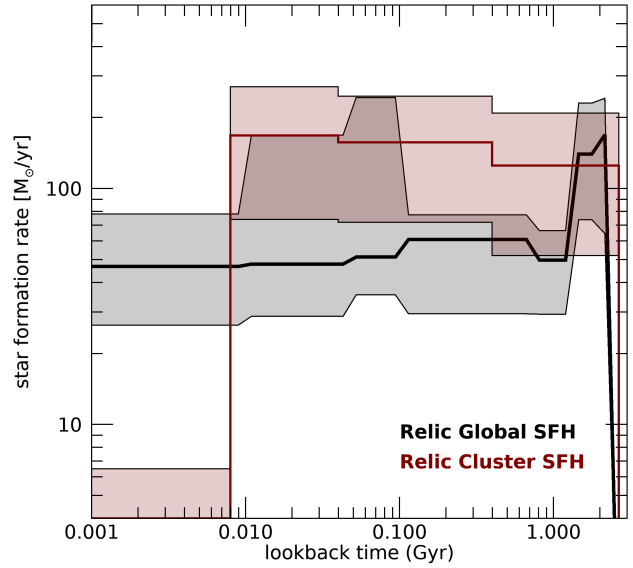


Figure 6. The star formation history of the main galaxy (black) is broadly similar to the cluster-inferred SFH (maroon). The cluster-implied SFR is ~ 2 - $3\times$ higher for lookback times < 1 Gyr, albeit still consistent within the large uncertainties. Our favored interpretation is that this excess supports a scenario where some fraction of the young and intermediate age clusters were accreted from the rich overdensity the Relic resides within.

The oldest clusters, which also have the largest stellar masses, only survive such long timescales if they are gravitationally bound. It is expected that these clusters will continue to shed mass through 2-body interactions as they evolve to the present day. Simulations predict up to an order of magnitude loss in stellar mass (e.g. Pfeffer et al. 2024), representing a trajectory in the age-mass plane that could naturally evolve the oldest Relic clusters to the present-day GC population. Given their high masses, it is therefore logical to speculate that the GCs in the Relic will survive evaporation driven by 2-body relaxation for the age of the universe. The Pfeffer et al. (2024) simulations presented in Figure 5 also nicely demonstrate how we are only seeing the ‘tip of the iceberg’, with the bulk of cluster population well below our detection limit.

While spectroscopy is needed to robustly constrain metallicity, our photometric analysis tentatively suggests that the older clusters have higher metallicities of order $\log(Z/Z_\odot) \sim -0.5$, whereas the younger clusters have metallicities ~ 1 dex lower with $\log(Z/Z_\odot) \sim -1.5$. The typical posterior ranges up to 0.5 dex in width for ages less than 500 Myr, but is a factor of 2 larger for older clusters where the age-metallicity degeneracy hinders interpretation. All clusters have metallicities closer to the 25% Solar metallicity trends relative to Solar metallicity, as shown in Figure 3, though there isn’t much distinguishing power with these particular colors. In

any case, both the young and old populations have inferred metallicities that would largely be considered “Population I” metal-rich clusters according to theoretical predictions (e.g., [Chen et al. 2024](#)). Given that the Relic resides in a massive dark matter halo, it is natural to expect the GCs to be dominated by Pop-I populations that formed through shock compression due to gravitational collapse, such as mergers ([Chen et al. 2024](#)). However, the metallicity prior does not extend below -2 and thus our analysis is not sensitive to recovering metal-poor clusters by not allowing for such solutions. Furthermore, in the absence of spectroscopy, these metallicity measurements should be interpreted with caution. The JWST/IFU spectroscopy will provide better constraints on metallicity in order to distinguish formation scenarios. We also note that we are not sensitive to detecting stellar sources in the core of the Relic, where they may have higher metallicities. The central diffuse light of the host galaxy when adopting a non-parametric star formation history and a mass-metallicity prior following [Gallazzi et al. \(2005\)](#) is overall metal-rich, with $\log(Z/Z_{\odot}) = 0.07 + 0.09_{-0.17}$.

The Relic exists in a known overdensity ([Naidu et al. 2024](#)), which laid the groundwork with a rich history prior to the epoch of observation. The Relic environment likely fueled past episodes of in-situ star formation and increased the probability of accretion events and dynamical interactions. The age and mass distributions of cluster systems in local galaxies are known to closely trace the past major star formation episodes, correlating with inferred star formation histories of the host galaxies (e.g., [Chandar et al. 2017, 2021](#)). In the case of the Relic, the clusters suggest three episodes of star formation (see Figure 5). If we assume a typical space velocity of 700 km/s for a galaxy in a proto-cluster and adopt a projected distance of 70 kpc to the nearest companion, this suggests the Relic flew by roughly 100 Myrs ago. In this context, the intermediate-age population of stellar clusters may have formed at least in part as the result of this particular interaction (more discussion in Section 5.2). In principle, we would expect to see a similar rejuvenation in the host galaxy light, however the uncertainties in the SFH are too large to reach a definitely conclusion (Figure 6). On the other hand, the oldest clusters are consistent with the mass-weighted age of the Relic, likely forming in tandem with the main stellar population.

5.2. Formation History of the Relic and its Clusters

While our ability to draw inferences directly from a photometry-based star formation history are limited, there is suggestive evidence from the diffuse host galaxy light that somewhat tells the same story as the cluster population. As described in Section 3.2, the SED of the main galaxy represents the spectral shape within the inner 0.5 arcseconds but is corrected to total through aperture corrections. This has

become a standard approach in the literature. As the light is completely distinct from the clump population, the resulting SFH serves as an interesting comparison point.

The SFH of the Relic in Figure 6 shows a main epoch of star formation 1-2 Gyr ago, with a relatively flat star formation history thereafter, with a star formation rate of $50 M_{\odot} \text{ yr}^{-1}$. An enhancement coinciding with the dynamical interaction with the two neighbors ~ 100 Myr in the past is only hinted at via the larger uncertainties at this epoch. For comparison, we also estimate a cluster-based star formation history. In short, we use the stellar masses of the clusters in the different age intervals together with observed local star formation rate (SFR)- cluster mass scaling relations to infer the SFR associated with each cluster ([Chandar et al. 2021](#)). This is then integrated based on all of the clumps within that age (lookback time) bin, resulting in a cluster-inferred SFH (maroon line in Figure 6). The caveat here is the unknown applicability of local scaling relations at high redshift – we expect significant progress in this area in the coming decade. In the following paragraphs, we discuss the similarities and differences between these two SFHs in the context of the observations as a whole in order to piece together the possible story of the Relic.

The main host galaxy SFH may support an interpretation where the young star clusters formed in tandem with the main galaxy owing to the ongoing lower-level star formation. The evidence for this ongoing star formation in the main galaxy comes from the moderate rest-UV light. The formation of young clusters may also be a natural outcome in the aftermath of the dynamical interaction if the Relic accreted new cold gas. However, there exists a discrepancy between the cluster- and galaxy-inferred SFHs (more on this below). Moreover, it is an open question as to how clusters get out into the halo. It has been suggested that clusters can form in a proto-disk and then be ejected into the halo due to violent relaxation ([Toomre & Toomre 1972](#)). While mergers can drive this violent relaxation, galaxies which experience such a recent merger would generally also show morphological disturbances (e.g., [Toomre & Toomre 1972](#); [Barnes 1998](#); [Mihos & Hernquist 1994](#); [Goudfrooij et al. 2007](#)) rather than presenting as a smooth elliptical galaxy. While there does exist a hint of a red tidal arc (see Figure 2) and a prominent stream of stars in the wake of the Relic, there is otherwise no obvious evidence for a recent major merger. Moreover, we do not see compelling evidence for a disk-like structure in the Relic. That said, we cannot rule out the presence of a disk from morphology alone given the existence of fast-rotating early-type galaxies at both $z \sim 0$ ([Cappellari 2016](#); [Graham et al. 2018](#)) and $z \sim 2$ ([Newman et al. 2018](#)).

Instead, it may be that the young to intermediate age clusters hold the best clues to the Relic’s formation history: despite the systemic quenching of the galaxy roughly one bil-

lion years prior (black line, Figure 6), it appears that clusters continued to form. This robust cluster population indicates an SFR that is $\approx 2-3$ times higher than the integrated light (with large uncertainties). So while it is logical to infer that the clusters closest to the tidal tail formed as a result of the past dynamical interaction, it is hard to explain halo clusters with a similar age. These ~ 100 Myr clusters, shown in the center panel of Figure 4 as white circles, are distributed throughout the halo of the Relic. The ejection scenario described above does not seem plausible. Another possible explanation is that these clusters have been accreted from smaller, nearby galaxies, which are common in the dense environment surrounding the Relic. A number of the halo globular clusters in the Milky Way have been accreted in this way (e.g., Brodie & Strader 2006; Forbes & Bridges 2010; Ishchenko et al. 2023; Belokurov & Kravtsov 2024). Moreover, local elliptical galaxies in dense environments are believed to accrete a significant fraction of their globular cluster populations (e.g., Brodie & Strader 2006). The lower metallicities found for these clusters only serves to further bolster this accretion hypothesis (see Section 5.1). It is therefore the notable gap at lookback times less than 1 Gyr between the cluster-based and main galaxy SFH together with the spatial distribution and lower metallicities of these young to intermediate age clusters that builds the case for an accretion origin. While speculative, this accretion interpretation also fits nicely into the larger hierarchical framework of galaxy formation, where the outskirts of quiescent galaxies show empirical evidence of significant growth over their subsequent many billions of years of evolution (e.g., van Dokkum et al. 2010; Hill et al. 2017). While the bulk of star formation happened in the distant past in the Relic, it will continue to evolve through minor mergers and accretion – tentatively supported herein by the existence of these young and intermediate age halo clusters.

All together, we see evidence for an age spread of ~ 2 Gyr for the GCs in this massive elliptical galaxy. While we present possible interpretations above, photometric uncertainties preclude a more definitive answer as to if these clusters formed in different bursts, more continuously, and/or if some fraction were accreted. The follow-up ultra-deep spectroscopic data (JWST-GO-2561) will provide more information regarding the true formation history of the clusters within the Relic.

Finally, it is worth noting that given the large stellar masses of the oldest clusters associated with the Relic, there may be alternative explanations worth exploring in future work. They may not be GCs at all, but rather ultra-compact dwarf galaxies that form through a previously unrecognized formation channel. Or perhaps the Relic is atypical in that its GC population has an usually top heavy GC mass function (e.g., some local examples in dwarf galaxies include van Dokkum

et al. 2018; Li et al. 2024). While it is common to invoke substantial mass loss between $z = 2.5$ at $z = 0$ as a solution, there may be something else at play in these high redshift galaxies yet to be understood.

5.3. Comparison with Theoretical Predictions

The E-MOSAICS project (MOdelling Star cluster population Assembly In Cosmological Simulations within EAGLE) offers cosmological hydrodynamical simulations of galaxy formation which allow for the formation and evolution of star clusters using subgrid models (Pfeffer et al. 2018; Kruijssen et al. 2019). Following their formation, clusters in the simulation lose mass due to stellar evolution, two-body relaxation, and shocks from rapidly changing tidal fields. Both young and old star clusters are assumed to form and evolve following the same physical mechanisms. The predicted ages and masses of clusters from the fiducial model of Pfeffer et al. (2024) at $z = 2.5$ are shown in grayscale in Figure 5, with the most extreme cluster masses (at different ages) plotted as the small gray circles. Our mass and age estimates for clusters in the Relic fall at the extreme upper end of the model predictions at a redshift of $z = 2.5$.

While significant mass-loss may not be necessary given the high mass clusters found in nearby post-merger systems (e.g., Schweizer & Seitzer 1998, 2007; He et al. 2022), we can make a very rough estimate of the expected mass loss following Pozzetti et al. (2019), where the number of bright clusters at high redshift directly scales with the implied mass loss. As we detect 27 globular clusters brighter than 30th magnitude, we might expect a subsequent mass loss of around 0.4 dex by $z = 0$. This number compares well to the results of Pfeffer et al. (2024), where the 70% of clusters that survive disruption lose 0.27 dex stellar mass on average from $z = 2.5$ to $z = 0$.

5.4. Comparison with High Redshift Cluster Observations

In Figure 7, we compare the properties of the clusters in the Relic with those determined for other high-redshift, lensed galaxies. Figure 7a shows the age of each cluster with redshift, with the literature compilation of observed stellar sources presented in Pfeffer et al. (2024). The Relic is shown by the maroon circles. Here we see that the ages of the clusters in the Relic are among the oldest identified thus far for any high-redshift galaxy. Figure 7b shows the formation redshift of the clusters relative to their stellar mass. While the Relic includes a relatively older population of clusters with earlier formation redshifts, the general range of stellar masses is similar to other measurements at high redshift. However, the Relic is unique among these galaxies in that it is an early-type galaxy, whereas the others are clearly later-type systems with on-going star formation. Taken at face value, this indicates that elliptical galaxies started to form stars and clusters

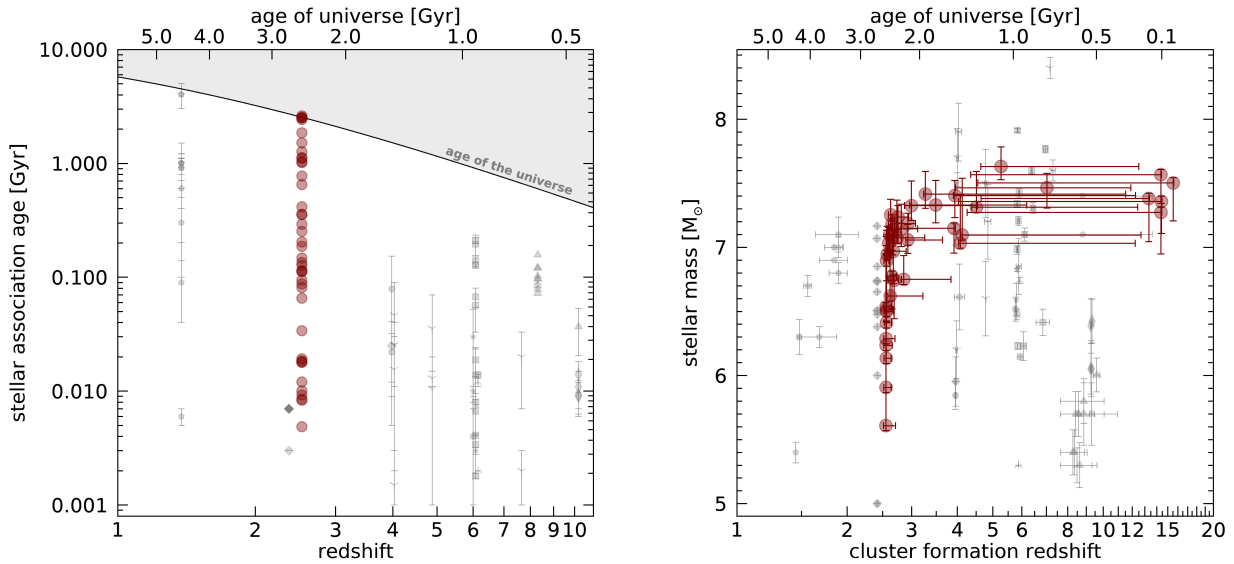


Figure 7. Compilation of mass, age, and associated formation redshift estimates for compact stellar sources discovered in lensed high-redshift galaxies with JWST photometry from Pfeffer et al. (2024): Cosmic Gems (thin diamond; Adamo et al. 2024), Firefly Sparkle (triangle; Mowla et al. 2024), MACS0416 (upward triangle; Messa et al. 2024a), Sunrise (star; Vanzella et al. 2023), Cosmic Grapes (square; Fujimoto et al. 2024), A2744 (circle; Vanzella et al. 2022a), Sparkler (pentagon; Mowla et al. 2022), RCS0224 and MACS0940 (downward triangle; Messa et al. 2024b). Plus one additional set of data based on HST photometry: Sunburst (diamond; Vanzella et al. 2022b). The Relic cluster age, formation redshift, and mass estimates are shown as maroon circles for comparison.

earlier than most gas-rich disk galaxies. This is also consistent with the dense environment where the Relic resides and the downsizing paradigm of galaxy formation as a whole (Thomas et al. 2005, 2010).

5.5. Link to Exotic Populations

Beyond their relationship to galaxy assembly, gravitationally bound, compact collections of stars that comprise GCs are also known to produce exotic stellar populations (Gratton et al. 2019). Dynamical interactions within GCs give rise to exotic systems, including X-ray binaries, pulsars, fast radio bursts, and merging BH systems (Giesler et al. 2018; Ivanova et al. 2008). The rate of binary black hole (BBH) mergers originating from GCs carries information about their abundance in the early universe, as well as their mass and radius distributions. It is thought that more massive, compact GCs give rise to more BBHs (Fishbach & Fragione 2023). While current GW detectors only reach $z \sim 1$, planned upgrades will extend detection to $z > 2$ within the next few years (Evans et al. 2021; Kalogera et al. 2019). If candidate massive clusters identified by JWST at high redshift were to survive a Hubble time, this would make them the progenitors of the local, metal-poor GCs that are factories for BBH mergers. While most clusters in the Relic won't be old enough yet, the most massive, metal-poor clusters may already be marking the first sites of BBH production, with GW signatures detectable in the near future.

6. CONCLUSIONS

In this paper, we overview the physical properties of 42 compact stellar sources, likely star clusters, associated with a massive, quiescent galaxy at $z = 2.53$ behind the Abell 2744 galaxy cluster. The clusters tell a story of the formation history of the Relic that provides a unique laboratory for testing globular cluster formation theories. Below we summarize the main results,

- The stellar populations of the Relic clusters are comprised of three main age groups. The oldest stars > 1 Gyr likely formed in-situ at $z > 5$ in tandem with the bulk of the host galaxy. The intermediate-age population, with ages of ~ 100 -500 Myr, are thought to be the result of both a tidal interaction with two nearby low-mass quiescent galaxies as well as clusters formed ex-situ and acquired via accretion events. While the galaxy is overall quenched, we see clear evidence for a young cluster population (10-100 Myr) that exist system wide spatially and are also suspected to have been accreted. Altogether, if the 42 clumps survive to the present day, they bookend the typical age range of local globular cluster systems of 11-13 Gyr.
- The Relic hosts over a dozen clusters that are sufficiently old to be considered both gravitationally-bound and likely to survive subsequent mass loss due to dynamic interactions. These clusters are the best known examples of globular cluster candidates at high redshift, given the combination of their old ages, compact/unresolved sizes, and moderately high

stellar masses. Moreover, they are the oldest clusters observed to date at similar redshifts, and unique in that their host galaxy is globally quenched already by $z = 2.5$.

- The stellar masses of the oldest clusters are of order $\log(M/M_{\odot}) \sim 7.5$, consistent with the largest formed globular clusters in model predictions. Over the subsequent 11 Gyr to the present-day, it is thought that these compact, gravitationally-bound stellar systems could experience up to an order of magnitude loss in stellar mass due to dynamical interactions.

The overdensity within which the Relic resides was discovered in one of the deepest, most homogeneous JWST datasets to date. This data will continue to serve as a fertile playground to search for clusters surrounding a wide range in host galaxy type and mass (e.g., see [Claeyssens et al. 2024](#)), presenting a unique opportunity to test globular cluster formation scenarios. In particular, globular clusters exist with high specific frequencies in both the lowest and highest mass quenched galaxies in the local universe ([Olsen et al. 2004](#); [Peng et al. 2008](#)). These massive quiescent galaxies form rapidly and shut down as early as $z \sim 5$ ([Carnall et al. 2023](#); [de Graaff et al. 2024](#); [Kakimoto et al. 2024](#); [Antwi-Danso et al. 2025](#)), whereas at least some fraction of the lower mass quiescent population quenches at slightly later times closer to $z \sim 1-2$ ([Cutler et al. 2024](#)). In either case, studies of the globular cluster populations within these galaxies need to push to $z > 2$ in order to distinguish in-situ formation versus accretion scenarios. Studies of rich overdensities of quiescent galaxies at cosmic noon will therefore enable us to draw evolutionary connections with globular cluster formation theories for larger samples. Moreover, there exist even deeper programs (e.g., JWST-GO-3293, PIs: Atek & Chisholm), where studies of the globular cluster luminosity function can be pushed even lower. The field is rapidly evolving, as evidenced by the sheer number of papers that have appeared in the literature on this topic in the last year alone, and thus this is merely a jumping off point to understand the formation of one of the most enigmatic populations that have long lurked in the halos and at the hearts of galaxies.

ACKNOWLEDGMENTS

This work is based in part on observations made with the NASA/ESA/CSA James Webb Space Telescope and the NASA/ESA Hubble Space Telescope obtained from the Space Telescope Science Institute, which is operated by the Association of Universities for Research in Astronomy, Inc., under NASA contract NAS 5-26555. The data were obtained from the Mikulski Archive for Space Telescopes at the Space Telescope Science Institute, which is operated by the Association of Universities for Research in Astronomy, Inc., under NASA contract NAS 5-03127 for JWST. These observations are associated with programs JWST-GO-2561, JWST-GO-4111, JWST-ERS-1324, JWST-DD-2756, HST-GO-11689, HST-GO-13386, HST-GO/DD-13495, HST-GO-13389, HST-GO-15117, and HST-GO/DD-17231. Support for programs JWST-GO-2561 and JWST-GO-4111 was provided by NASA through a grant from the Space Telescope Science Institute, which is operated by the Associations of Universities for Research in Astronomy, Incorporated, under NASA contract NAS 5-03127. Some of the data products presented herein were retrieved from the Dawn JWST Archive (DJA). DJA is an initiative of the Cosmic Dawn Center, which is funded by the Danish National Research Foundation under grant No. 140. AZ acknowledges support by Grant No. 2020750 from the United States-Israel Binational Science Foundation (BSF) and Grant No. 2109066 from the United States National Science Foundation (NSF); and by the Israel Science Foundation Grant No. 864/23.

Facilities: JWST (NIRCam)

Software: ASTROPY ([Astropy Collaboration et al. 2013, 2018, 2022](#)), EA_zY ([Brammer et al. 2008](#)) GRIZLI ([Brammer 2023, \[github.com/gbrammer/grizli\]\(https://github.com/gbrammer/grizli\)](#)), GALFIT ([Peng et al. 2002, 2010b](#)), PROSPECTOR ([Johnson et al. 2021](#)), FSPS ([Conroy et al. 2009, 2010](#); [Conroy & Gunn 2010](#)) PYTHON-FSPS ([Foreman-Mackey et al. \(2014\)](#)) APERPY ([Weaver et al. 2024, \[github.com/astrowhit/aperpy\]\(https://github.com/astrowhit/aperpy\)](#)) SOURCE EXTRACTOR ([Bertin & Arnouts 1996](#)), SEP ([Barbary 2016a](#)), EXTINCTION ([Barbary 2016b](#)), SFDMAP ([Schlegel et al. 1998](#); [Schlafly & Finkbeiner 2011, \[github.com/kbarbary/sfdmap\]\(https://github.com/kbarbary/sfdmap\)](#)), PYPHER ([Boucaud et al. 2016](#)), PHOTUTILS ([Bradley et al. 2022](#)), ASTRODRIZZLE ([Gonzaga et al. 2012](#)), NUMPY ([van der Walt et al. 2011](#)), MATPLOTLIB ([Hunter 2007](#))

REFERENCES

- Adamo, A., Usher, C., Pfeffer, J., & Claeyssens, A. 2023, MNRAS, 525, L6, doi: [10.1093/mnras/slad084](https://doi.org/10.1093/mnras/slad084)
- Adamo, A., Zeidler, P., Kruijssen, J. M. D., et al. 2020, SSRv, 216, 69, doi: [10.1007/s11214-020-00690-x](https://doi.org/10.1007/s11214-020-00690-x)
- Adamo, A., Bradley, L. D., Vanzella, E., et al. 2024, Nature, 632, 513, doi: [10.1038/s41586-024-07703-7](https://doi.org/10.1038/s41586-024-07703-7)
- Antwi-Danso, J., Papovich, C., Esdaile, J., et al. 2025, ApJ, 978, 90, doi: [10.3847/1538-4357/ad8b30](https://doi.org/10.3847/1538-4357/ad8b30)

- Ashman, K. M., & Zepf, S. E. 1992, *ApJ*, 384, 50, doi: [10.1086/170850](https://doi.org/10.1086/170850)
- Astropy Collaboration, Robitaille, T. P., Tollerud, E. J., et al. 2013, *A&A*, 558, A33, doi: [10.1051/0004-6361/201322068](https://doi.org/10.1051/0004-6361/201322068)
- Astropy Collaboration, Price-Whelan, A. M., Sipőcz, B. M., et al. 2018, *AJ*, 156, 123, doi: [10.3847/1538-3881/aabc4f](https://doi.org/10.3847/1538-3881/aabc4f)
- Astropy Collaboration, Price-Whelan, A. M., Lim, P. L., et al. 2022, *apj*, 935, 167, doi: [10.3847/1538-4357/ac7c74](https://doi.org/10.3847/1538-4357/ac7c74)
- Atek, H., Labbé, I., Furtak, L. J., et al. 2024, *Nature*, 626, 975, doi: [10.1038/s41586-024-07043-6](https://doi.org/10.1038/s41586-024-07043-6)
- Barbary, K. 2016a, *The Journal of Open Source Software*, 1, 58, doi: [10.21105/joss.00058](https://doi.org/10.21105/joss.00058)
- . 2016b, *extinction v0.3.0*, Zenodo, doi: [10.5281/zenodo.804967](https://doi.org/10.5281/zenodo.804967)
- Barnes, J. E. 1998, in *Saas-Fee Advanced Course 26: Galaxies: Interactions and Induced Star Formation*, ed. R. C. Kennicutt, Jr., F. Schweizer, J. E. Barnes, D. Friedli, L. Martinet, & D. Pfenniger, 275
- Beasley, M. A., Baugh, C. M., Forbes, D. A., Sharples, R. M., & Frenk, C. S. 2002, *MNRAS*, 333, 383, doi: [10.1046/j.1365-8711.2002.05402.x](https://doi.org/10.1046/j.1365-8711.2002.05402.x)
- Beaulieu, S. F., Gilmore, G., Elson, R. A. W., et al. 2001, *AJ*, 121, 2618, doi: [10.1086/320371](https://doi.org/10.1086/320371)
- Belokurov, V., & Kravtsov, A. 2024, *MNRAS*, 528, 3198, doi: [10.1093/mnras/stad3920](https://doi.org/10.1093/mnras/stad3920)
- Bergamini, P., Acebron, A., Grillo, C., et al. 2023, *A&A*, 670, A60, doi: [10.1051/0004-6361/202244575](https://doi.org/10.1051/0004-6361/202244575)
- Bertin, E., & Arnouts, S. 1996, *A&AS*, 117, 393, doi: [10.1051/aas:1996164](https://doi.org/10.1051/aas:1996164)
- Bezanson, R., Labbe, I., Whitaker, K. E., et al. 2024, *ApJ*, 974, 92, doi: [10.3847/1538-4357/ad66cf](https://doi.org/10.3847/1538-4357/ad66cf)
- Boucaud, A., Bocchio, M., Abergel, A., et al. 2016, *A&A*, 596, A63, doi: [10.1051/0004-6361/201629080](https://doi.org/10.1051/0004-6361/201629080)
- Bradley, L., Sipőcz, B., Robitaille, T., et al. 2022, *astropy/photutils: 1.5.0*, Zenodo, doi: [10.5281/zenodo.6825092](https://doi.org/10.5281/zenodo.6825092)
- . 2024, *astropy/photutils: 2.0.2*, Zenodo, doi: [10.5281/zenodo.596036](https://doi.org/10.5281/zenodo.596036)
- Brammer, G. 2023, *grizli*, 1.9.11, Zenodo, doi: [10.5281/zenodo.8370018](https://doi.org/10.5281/zenodo.8370018)
- Brammer, G. B., van Dokkum, P. G., & Coppi, P. 2008, *ApJ*, 686, 1503, doi: [10.1086/591786](https://doi.org/10.1086/591786)
- Brodie, J. P., & Strader, J. 2006, *ARA&A*, 44, 193, doi: [10.1146/annurev.astro.44.051905.092441](https://doi.org/10.1146/annurev.astro.44.051905.092441)
- Brodie, J. P., Usher, C., Conroy, C., et al. 2012, *ApJL*, 759, L33, doi: [10.1088/2041-8205/759/2/L33](https://doi.org/10.1088/2041-8205/759/2/L33)
- Bruzual, G., & Charlot, S. 2003, *MNRAS*, 344, 1000, doi: [10.1046/j.1365-8711.2003.06897.x](https://doi.org/10.1046/j.1365-8711.2003.06897.x)
- Cappellari, M. 2016, *ARA&A*, 54, 597, doi: [10.1146/annurev-astro-082214-122432](https://doi.org/10.1146/annurev-astro-082214-122432)
- Carnall, A. C., McLure, R. J., Dunlop, J. S., et al. 2023, *Nature*, 619, 716, doi: [10.1038/s41586-023-06158-6](https://doi.org/10.1038/s41586-023-06158-6)
- Chabrier, G. 2003, *PASP*, 115, 763, doi: [10.1086/376392](https://doi.org/10.1086/376392)
- Chandar, R., Fall, S. M., Whitmore, B. C., & Mulia, A. J. 2017, *ApJ*, 849, 128, doi: [10.3847/1538-4357/aa92ce](https://doi.org/10.3847/1538-4357/aa92ce)
- Chandar, R., Mok, A., French, K. D., Smercina, A., & Smith, J.-D. T. 2021, *ApJ*, 920, 105, doi: [10.3847/1538-4357/ac0c19](https://doi.org/10.3847/1538-4357/ac0c19)
- Chandar, R., Caputo, M., Mok, A., et al. 2023, *ApJ*, 949, 116, doi: [10.3847/1538-4357/acc93b](https://doi.org/10.3847/1538-4357/acc93b)
- Charlot, S., & Fall, S. M. 2000, *ApJ*, 539, 718, doi: [10.1086/309250](https://doi.org/10.1086/309250)
- Chen, Y., Mo, H., & Wang, H. 2024, *arXiv e-prints*, arXiv:2405.18735, doi: [10.48550/arXiv.2405.18735](https://doi.org/10.48550/arXiv.2405.18735)
- Choi, J., Dotter, A., Conroy, C., et al. 2016, *ApJ*, 823, 102, doi: [10.3847/0004-637X/823/2/102](https://doi.org/10.3847/0004-637X/823/2/102)
- Claeysens, A., Adamo, A., Messa, M., et al. 2024, *arXiv e-prints*, arXiv:2410.10974, doi: [10.48550/arXiv.2410.10974](https://doi.org/10.48550/arXiv.2410.10974)
- Claeysens, A., Adamo, A., Richard, J., et al. 2023, *MNRAS*, 520, 2180, doi: [10.1093/mnras/stac3791](https://doi.org/10.1093/mnras/stac3791)
- Conroy, C., & Gunn, J. E. 2010, *ApJ*, 712, 833, doi: [10.1088/0004-637X/712/2/833](https://doi.org/10.1088/0004-637X/712/2/833)
- Conroy, C., Gunn, J. E., & White, M. 2009, *ApJ*, 699, 486, doi: [10.1088/0004-637X/699/1/486](https://doi.org/10.1088/0004-637X/699/1/486)
- Conroy, C., White, M., & Gunn, J. E. 2010, *ApJ*, 708, 58, doi: [10.1088/0004-637X/708/1/58](https://doi.org/10.1088/0004-637X/708/1/58)
- Côté, P., Marzke, R. O., & West, M. J. 1998, *ApJ*, 501, 554, doi: [10.1086/305838](https://doi.org/10.1086/305838)
- Cutler, S. E., Whitaker, K. E., Mowla, L. A., et al. 2022, *ApJ*, 925, 34, doi: [10.3847/1538-4357/ac341c](https://doi.org/10.3847/1538-4357/ac341c)
- Cutler, S. E., Whitaker, K. E., Weaver, J. R., et al. 2024, *ApJL*, 967, L23, doi: [10.3847/2041-8213/ad464c](https://doi.org/10.3847/2041-8213/ad464c)
- De Angeli, F., Piotto, G., Cassisi, S., et al. 2005, *AJ*, 130, 116, doi: [10.1086/430723](https://doi.org/10.1086/430723)
- de Graaff, A., Setton, D. J., Brammer, G., et al. 2024, *Nature Astronomy*, doi: [10.1038/s41550-024-02424-3](https://doi.org/10.1038/s41550-024-02424-3)
- de la Fuente Marcos, R., de la Fuente Marcos, C., Moni Bidin, C., Ortolani, S., & Carraro, G. 2015, *A&A*, 581, A13, doi: [10.1051/0004-6361/201526580](https://doi.org/10.1051/0004-6361/201526580)
- De Lucia, G., Kruijssen, J. M. D., Trujillo-Gomez, S., Hirschmann, M., & Xie, L. 2024, *MNRAS*, 530, 2760, doi: [10.1093/mnras/stae1006](https://doi.org/10.1093/mnras/stae1006)
- Dolfi, A., Forbes, D. A., Couch, W. J., et al. 2021, *MNRAS*, 504, 4923, doi: [10.1093/mnras/stab1023](https://doi.org/10.1093/mnras/stab1023)
- Dotter, A. 2016, *ApJS*, 222, 8, doi: [10.3847/0067-0049/222/1/8](https://doi.org/10.3847/0067-0049/222/1/8)
- Evans, M., Adhikari, R. X., Afle, C., et al. 2021, *arXiv e-prints*, arXiv:2109.09882, doi: [10.48550/arXiv.2109.09882](https://doi.org/10.48550/arXiv.2109.09882)
- Faifer, F. R., Forte, J. C., Norris, M. A., et al. 2011, *MNRAS*, 416, 155, doi: [10.1111/j.1365-2966.2011.19018.x](https://doi.org/10.1111/j.1365-2966.2011.19018.x)
- Fishbach, M., & Fragione, G. 2023, *MNRAS*, 522, 5546, doi: [10.1093/mnras/stad1364](https://doi.org/10.1093/mnras/stad1364)
- Forbes, D. A., & Bridges, T. 2010, *MNRAS*, 404, 1203, doi: [10.1111/j.1365-2966.2010.16373.x](https://doi.org/10.1111/j.1365-2966.2010.16373.x)

- Forbes, D. A., Brodie, J. P., & Grillmair, C. J. 1997, *AJ*, 113, 1652, doi: [10.1086/118382](https://doi.org/10.1086/118382)
- Forbes, D. A., & Remus, R.-S. 2018, *MNRAS*, 479, 4760, doi: [10.1093/mnras/sty1767](https://doi.org/10.1093/mnras/sty1767)
- Foreman-Mackey, D., Sick, J., & Johnson, B. 2014, python-fsps: Python bindings to FSPS (v0.1.1), v0.1.1, Zenodo, doi: [10.5281/zenodo.12157](https://doi.org/10.5281/zenodo.12157)
- Förster Schreiber, N. M., Shapley, A. E., Genzel, R., et al. 2011, *ApJ*, 739, 45, doi: [10.1088/0004-637X/739/1/45](https://doi.org/10.1088/0004-637X/739/1/45)
- Fujimoto, S., Ouchi, M., Kohno, K., et al. 2024, arXiv e-prints, arXiv:2402.18543, doi: [10.48550/arXiv.2402.18543](https://doi.org/10.48550/arXiv.2402.18543)
- Furtak, L. J., Zitrin, A., Weaver, J. R., et al. 2023, *MNRAS*, 523, 4568, doi: [10.1093/mnras/stad1627](https://doi.org/10.1093/mnras/stad1627)
- Gallazzi, A., Charlot, S., Brinchmann, J., White, S. D. M., & Tremonti, C. A. 2005, *MNRAS*, 362, 41, doi: [10.1111/j.1365-2966.2005.09321.x](https://doi.org/10.1111/j.1365-2966.2005.09321.x)
- Gardner, J. P., Mather, J. C., Abbott, R., et al. 2023, *PASP*, 135, 068001, doi: [10.1088/1538-3873/acd1b5](https://doi.org/10.1088/1538-3873/acd1b5)
- Giesler, M., Clausen, D., & Ott, C. D. 2018, *MNRAS*, 477, 1853, doi: [10.1093/mnras/sty659](https://doi.org/10.1093/mnras/sty659)
- Glazebrook, K., Nanayakkara, T., Schreiber, C., et al. 2024, *Nature*, 628, 277, doi: [10.1038/s41586-024-07191-9](https://doi.org/10.1038/s41586-024-07191-9)
- Gonzaga, S., Hack, W., Fruchter, A., & Mack, J. 2012, *The DrizzlePac Handbook*
- Goudfrooij, P., Alonso, M. V., Maraston, C., & Minniti, D. 2001, *MNRAS*, 328, 237, doi: [10.1046/j.1365-8711.2001.04860.x](https://doi.org/10.1046/j.1365-8711.2001.04860.x)
- Goudfrooij, P., Schweizer, F., Gilmore, D., & Whitmore, B. C. 2007, *AJ*, 133, 2737, doi: [10.1086/516634](https://doi.org/10.1086/516634)
- Graham, M. T., Cappellari, M., Li, H., et al. 2018, *MNRAS*, 477, 4711, doi: [10.1093/mnras/sty504](https://doi.org/10.1093/mnras/sty504)
- Gratton, R., Bragaglia, A., Carretta, E., et al. 2019, *A&A Rv*, 27, 8, doi: [10.1007/s00159-019-0119-3](https://doi.org/10.1007/s00159-019-0119-3)
- Guo, Y., Gialvalisco, M., Ferguson, H. C., Cassata, P., & Koekemoer, A. M. 2012, *ApJ*, 757, 120, doi: [10.1088/0004-637X/757/2/120](https://doi.org/10.1088/0004-637X/757/2/120)
- Guo, Y., Ferguson, H. C., Bell, E. F., et al. 2015, *ApJ*, 800, 39, doi: [10.1088/0004-637X/800/1/39](https://doi.org/10.1088/0004-637X/800/1/39)
- Guo, Y., Rafelski, M., Bell, E. F., et al. 2018, *ApJ*, 853, 108, doi: [10.3847/1538-4357/aaa018](https://doi.org/10.3847/1538-4357/aaa018)
- Harris, W. E. 1996, *AJ*, 112, 1487, doi: [10.1086/118116](https://doi.org/10.1086/118116)
- Harris, W. E., Harris, G. L., & Hudson, M. J. 2015, *ApJ*, 806, 36, doi: [10.1088/0004-637X/806/1/36](https://doi.org/10.1088/0004-637X/806/1/36)
- Harris, W. E., & Reina-Campos, M. 2023, *MNRAS*, 526, 2696, doi: [10.1093/mnras/stad2903](https://doi.org/10.1093/mnras/stad2903)
- He, H., Wilson, C., Brunetti, N., et al. 2022, *ApJ*, 928, 57, doi: [10.3847/1538-4357/ac5628](https://doi.org/10.3847/1538-4357/ac5628)
- Hilker, M., Infante, L., & Richtler, T. 1999, *A&AS*, 138, 55, doi: [10.1051/aas:1999495](https://doi.org/10.1051/aas:1999495)
- Hill, A. R., Muzzin, A., Franx, M., et al. 2017, *ApJ*, 837, 147, doi: [10.3847/1538-4357/aa61fe](https://doi.org/10.3847/1538-4357/aa61fe)
- Hopkins, P. F., Cox, T. J., Younger, J. D., & Hernquist, L. 2009, *ApJ*, 691, 1168, doi: [10.1088/0004-637X/691/2/1168](https://doi.org/10.1088/0004-637X/691/2/1168)
- Hunter, J. D. 2007, *Computing in Science and Engineering*, 9, 90, doi: [10.1109/MCSE.2007.55](https://doi.org/10.1109/MCSE.2007.55)
- Ishchenko, M., Sobolenko, M., Berczik, P., et al. 2023, *A&A*, 673, A152, doi: [10.1051/0004-6361/202245117](https://doi.org/10.1051/0004-6361/202245117)
- Ivanova, N., Heinke, C. O., Rasio, F. A., Belczynski, K., & Fregeau, J. M. 2008, *MNRAS*, 386, 553, doi: [10.1111/j.1365-2966.2008.13064.x](https://doi.org/10.1111/j.1365-2966.2008.13064.x)
- Johnson, B. D., Leja, J., Conroy, C., & Speagle, J. S. 2021, *ApJS*, 254, 22, doi: [10.3847/1538-4365/abef67](https://doi.org/10.3847/1538-4365/abef67)
- Jordán, A., Côté, P., Blakeslee, J. P., et al. 2005, *ApJ*, 634, 1002, doi: [10.1086/497092](https://doi.org/10.1086/497092)
- Kakimoto, T., Tanaka, M., Onodera, M., et al. 2024, *ApJ*, 963, 49, doi: [10.3847/1538-4357/ad1ff1](https://doi.org/10.3847/1538-4357/ad1ff1)
- Kalogera, V., Berry, C. P. L., Colpi, M., et al. 2019, *BAAS*, 51, 242, doi: [10.48550/arXiv.1903.09220](https://doi.org/10.48550/arXiv.1903.09220)
- Kissler-Patig, M. 2000, *Reviews in Modern Astronomy*, 13, 13, doi: [10.48550/arXiv.astro-ph/0002070](https://doi.org/10.48550/arXiv.astro-ph/0002070)
- Kluge, M., Remus, R.-S., Babyk, I. V., Forbes, D. A., & Dolfi, A. 2023, *MNRAS*, 521, 4852, doi: [10.1093/mnras/stad882](https://doi.org/10.1093/mnras/stad882)
- Kriek, M., & Conroy, C. 2013, *ApJL*, 775, L16, doi: [10.1088/2041-8205/775/1/L16](https://doi.org/10.1088/2041-8205/775/1/L16)
- Kriek, M., van Dokkum, P. G., Franx, M., Illingworth, G. D., & Magee, D. K. 2009, *ApJL*, 705, L71, doi: [10.1088/0004-637X/705/1/L71](https://doi.org/10.1088/0004-637X/705/1/L71)
- Kriek, M., Conroy, C., van Dokkum, P. G., et al. 2016, *Nature*, 540, 248, doi: [10.1038/nature20570](https://doi.org/10.1038/nature20570)
- Kruijssen, J. M. D. 2014, *Classical and Quantum Gravity*, 31, 244006, doi: [10.1088/0264-9381/31/24/244006](https://doi.org/10.1088/0264-9381/31/24/244006)
- Kruijssen, J. M. D., Pfeffer, J. L., Crain, R. A., & Bastian, N. 2019, *MNRAS*, 486, 3134, doi: [10.1093/mnras/stz968](https://doi.org/10.1093/mnras/stz968)
- Krumholz, M. R., McKee, C. F., & Bland-Hawthorn, J. 2019, *ARA&A*, 57, 227, doi: [10.1146/annurev-astro-091918-104430](https://doi.org/10.1146/annurev-astro-091918-104430)
- Kundu, A., & Whitmore, B. C. 1998, *AJ*, 116, 2841, doi: [10.1086/300643](https://doi.org/10.1086/300643)
- Kundu, A., Whitmore, B. C., Sparks, W. B., et al. 1999, *ApJ*, 513, 733, doi: [10.1086/306865](https://doi.org/10.1086/306865)
- Lada, C. J., & Lada, E. A. 2003, *ARA&A*, 41, 57, doi: [10.1146/annurev.astro.41.011802.094844](https://doi.org/10.1146/annurev.astro.41.011802.094844)
- Laevens, B. P. M., Martin, N. F., Sesar, B., et al. 2014, *ApJL*, 786, L3, doi: [10.1088/2041-8205/786/1/L3](https://doi.org/10.1088/2041-8205/786/1/L3)
- Larsen, S. S., Brodie, J. P., Huchra, J. P., Forbes, D. A., & Grillmair, C. J. 2001, *AJ*, 121, 2974, doi: [10.1086/321081](https://doi.org/10.1086/321081)
- Leaman, R., VandenBerg, D. A., & Mendel, J. T. 2013, *MNRAS*, 436, 122, doi: [10.1093/mnras/stt1540](https://doi.org/10.1093/mnras/stt1540)
- Leja, J., Speagle, J. S., Ting, Y.-S., et al. 2022, *ApJ*, 936, 165, doi: [10.3847/1538-4357/ac887d](https://doi.org/10.3847/1538-4357/ac887d)
- Li, D., Eadie, G., Brown, P., et al. 2024, arXiv e-prints, arXiv:2409.06040, doi: [10.48550/arXiv.2409.06040](https://doi.org/10.48550/arXiv.2409.06040)

- Li, H., & Gnedin, O. Y. 2014, *ApJ*, 796, 10, doi: [10.1088/0004-637X/796/1/10](https://doi.org/10.1088/0004-637X/796/1/10)
- Mackey, A. D., & Gilmore, G. F. 2004, *MNRAS*, 355, 504, doi: [10.1111/j.1365-2966.2004.08343.x](https://doi.org/10.1111/j.1365-2966.2004.08343.x)
- Marín-Franch, A., Aparicio, A., Piotto, G., et al. 2009, *ApJ*, 694, 1498, doi: [10.1088/0004-637X/694/2/1498](https://doi.org/10.1088/0004-637X/694/2/1498)
- Messa, M., Dessauges-Zavadsky, M., Adamo, A., Richard, J., & Claeysens, A. 2024a, *MNRAS*, 529, 2162, doi: [10.1093/mnras/stae565](https://doi.org/10.1093/mnras/stae565)
- Messa, M., Vanzella, E., Loiacono, F., et al. 2024b, arXiv e-prints, arXiv:2407.20331, doi: [10.48550/arXiv.2407.20331](https://doi.org/10.48550/arXiv.2407.20331)
- Mihos, J. C., & Hernquist, L. 1994, *ApJL*, 431, L9, doi: [10.1086/187460](https://doi.org/10.1086/187460)
- Momany, Y., Ortolani, S., Held, E. V., et al. 2003, *A&A*, 402, 607, doi: [10.1051/0004-6361:20030295](https://doi.org/10.1051/0004-6361:20030295)
- Mowla, L., Iyer, K. G., Desprez, G., et al. 2022, *ApJL*, 937, L35, doi: [10.3847/2041-8213/ac90ca](https://doi.org/10.3847/2041-8213/ac90ca)
- Mowla, L., Iyer, K., Asada, Y., et al. 2024, arXiv e-prints, arXiv:2402.08696, doi: [10.48550/arXiv.2402.08696](https://doi.org/10.48550/arXiv.2402.08696)
- Naidu, R. P., Matthee, J., Kramarenko, I., et al. 2024, arXiv e-prints, arXiv:2410.01874, doi: [10.48550/arXiv.2410.01874](https://doi.org/10.48550/arXiv.2410.01874)
- Newman, A. B., Belli, S., Ellis, R. S., & Patel, S. G. 2018, *ApJ*, 862, 126, doi: [10.3847/1538-4357/aacd4f](https://doi.org/10.3847/1538-4357/aacd4f)
- Newton, O., Davies, J. J., Pfeffer, J., et al. 2024, arXiv e-prints, arXiv:2409.04516, doi: [10.48550/arXiv.2409.04516](https://doi.org/10.48550/arXiv.2409.04516)
- Oke, J. B. 1974, *ApJS*, 27, 21, doi: [10.1086/190287](https://doi.org/10.1086/190287)
- Olsen, K. A. G., Miller, B. W., Suntzeff, N. B., Schommer, R. A., & Bright, J. 2004, *AJ*, 127, 2674, doi: [10.1086/383297](https://doi.org/10.1086/383297)
- Peng, C. Y., Ho, L. C., Impey, C. D., & Rix, H.-W. 2002, *AJ*, 124, 266, doi: [10.1086/340952](https://doi.org/10.1086/340952)
- . 2010a, *AJ*, 139, 2097, doi: [10.1088/0004-6256/139/6/2097](https://doi.org/10.1088/0004-6256/139/6/2097)
- . 2010b, *AJ*, 139, 2097, doi: [10.1088/0004-6256/139/6/2097](https://doi.org/10.1088/0004-6256/139/6/2097)
- Peng, E. W., Ford, H. C., & Freeman, K. C. 2004, *ApJ*, 602, 705, doi: [10.1086/381236](https://doi.org/10.1086/381236)
- Peng, E. W., Jordán, A., Côté, P., et al. 2008, *ApJ*, 681, 197, doi: [10.1086/587951](https://doi.org/10.1086/587951)
- Pfeffer, J., Kruijssen, J. M. D., Bastian, N., Crain, R. A., & Trujillo-Gomez, S. 2023, *MNRAS*, 519, 5384, doi: [10.1093/mnras/stad044](https://doi.org/10.1093/mnras/stad044)
- Pfeffer, J., Kruijssen, J. M. D., Crain, R. A., & Bastian, N. 2018, *MNRAS*, 475, 4309, doi: [10.1093/mnras/stx3124](https://doi.org/10.1093/mnras/stx3124)
- Pfeffer, J., Janssens, S. R., Buzzo, M. L., et al. 2024, *MNRAS*, 529, 4914, doi: [10.1093/mnras/stae850](https://doi.org/10.1093/mnras/stae850)
- Pota, V., Forbes, D. A., Romanowsky, A. J., et al. 2013, *MNRAS*, 428, 389, doi: [10.1093/mnras/sts029](https://doi.org/10.1093/mnras/sts029)
- Pozzetti, L., Maraston, C., & Renzini, A. 2019, *MNRAS*, 485, 5861, doi: [10.1093/mnras/stz785](https://doi.org/10.1093/mnras/stz785)
- Sánchez-Blázquez, P., Peletier, R. F., Jiménez-Vicente, J., et al. 2006, *MNRAS*, 371, 703, doi: [10.1111/j.1365-2966.2006.10699.x](https://doi.org/10.1111/j.1365-2966.2006.10699.x)
- Schlafly, E. F., & Finkbeiner, D. P. 2011, *ApJ*, 737, 103, doi: [10.1088/0004-637X/737/2/103](https://doi.org/10.1088/0004-637X/737/2/103)
- Schlegel, D. J., Finkbeiner, D. P., & Davis, M. 1998, *ApJ*, 500, 525, doi: [10.1086/305772](https://doi.org/10.1086/305772)
- Schweizer, F., & Seitzer, P. 1998, *AJ*, 116, 2206, doi: [10.1086/300616](https://doi.org/10.1086/300616)
- . 2007, *AJ*, 133, 2132, doi: [10.1086/513317](https://doi.org/10.1086/513317)
- Speagle, J. S. 2020, *MNRAS*, 493, 3132, doi: [10.1093/mnras/staa278](https://doi.org/10.1093/mnras/staa278)
- Speagle, J. S., Steinhardt, C. L., Capak, P. L., & Silverman, J. D. 2014, *ApJS*, 214, 15, doi: [10.1088/0067-0049/214/2/15](https://doi.org/10.1088/0067-0049/214/2/15)
- Spitler, L. R., Larsen, S. S., Strader, J., et al. 2006, *AJ*, 132, 1593, doi: [10.1086/507328](https://doi.org/10.1086/507328)
- Strader, J., Brodie, J. P., Cenarro, A. J., Beasley, M. A., & Forbes, D. A. 2005, *AJ*, 130, 1315, doi: [10.1086/432717](https://doi.org/10.1086/432717)
- Suess, K. A., Weaver, J. R., Price, S. H., et al. 2024, *ApJ*, 976, 101, doi: [10.3847/1538-4357/ad75fe](https://doi.org/10.3847/1538-4357/ad75fe)
- Thomas, D., Maraston, C., Bender, R., & Mendes de Oliveira, C. 2005, *ApJ*, 621, 673, doi: [10.1086/426932](https://doi.org/10.1086/426932)
- Thomas, D., Maraston, C., Schawinski, K., Sarzi, M., & Silk, J. 2010, *MNRAS*, 404, 1775, doi: [10.1111/j.1365-2966.2010.16427.x](https://doi.org/10.1111/j.1365-2966.2010.16427.x)
- Toomre, A., & Toomre, J. 1972, *ApJ*, 178, 623, doi: [10.1086/151823](https://doi.org/10.1086/151823)
- Usher, C., Forbes, D. A., Brodie, J. P., et al. 2012, *MNRAS*, 426, 1475, doi: [10.1111/j.1365-2966.2012.21801.x](https://doi.org/10.1111/j.1365-2966.2012.21801.x)
- van der Walt, S., Colbert, S. C., & Varoquaux, G. 2011, *Computing in Science and Engineering*, 13, 22, doi: [10.1109/MCSE.2011.37](https://doi.org/10.1109/MCSE.2011.37)
- van Dokkum, P., Cohen, Y., Danieli, S., et al. 2018, *ApJL*, 856, L30, doi: [10.3847/2041-8213/aab60b](https://doi.org/10.3847/2041-8213/aab60b)
- van Dokkum, P. G., Whitaker, K. E., Brammer, G., et al. 2010, *ApJ*, 709, 1018, doi: [10.1088/0004-637X/709/2/1018](https://doi.org/10.1088/0004-637X/709/2/1018)
- Vanzella, E., Castellano, M., Bergamini, P., et al. 2022a, *ApJL*, 940, L53, doi: [10.3847/2041-8213/ac8c2d](https://doi.org/10.3847/2041-8213/ac8c2d)
- . 2022b, *A&A*, 659, A2, doi: [10.1051/0004-6361/202141590](https://doi.org/10.1051/0004-6361/202141590)
- Vanzella, E., Claeysens, A., Welch, B., et al. 2023, *ApJ*, 945, 53, doi: [10.3847/1538-4357/acb59a](https://doi.org/10.3847/1538-4357/acb59a)
- Wang, B., Leja, J., Bezanson, R., et al. 2023, *ApJL*, 944, L58, doi: [10.3847/2041-8213/acba99](https://doi.org/10.3847/2041-8213/acba99)
- Wang, B., Leja, J., Labbé, I., et al. 2024, *ApJS*, 270, 12, doi: [10.3847/1538-4365/ad0846](https://doi.org/10.3847/1538-4365/ad0846)
- Weaver, J. R., Cutler, S. E., Pan, R., et al. 2024, *ApJS*, 270, 7, doi: [10.3847/1538-4365/ad07e0](https://doi.org/10.3847/1538-4365/ad07e0)
- Welch, B., Coe, D., Zitrin, A., et al. 2023, *ApJ*, 943, 2, doi: [10.3847/1538-4357/aca8a8](https://doi.org/10.3847/1538-4357/aca8a8)
- Whitmore, B. C., Chandar, R., Lee, J., et al. 2020, *ApJ*, 889, 154, doi: [10.3847/1538-4357/ab59e5](https://doi.org/10.3847/1538-4357/ab59e5)
- Wuyts, S., Förster Schreiber, N. M., Genzel, R., et al. 2012, *ApJ*, 753, 114, doi: [10.1088/0004-637X/753/2/114](https://doi.org/10.1088/0004-637X/753/2/114)

Ying, J. M., Chaboyer, B., Boudreaux, E. M., et al. 2023, AJ, 166,
18, doi: [10.3847/1538-3881/acd9b1](https://doi.org/10.3847/1538-3881/acd9b1)
Ying, J. M., Chaboyer, B., & Du, W. 2024, ApJ, 970, 184,
doi: [10.3847/1538-4357/ad59a9](https://doi.org/10.3847/1538-4357/ad59a9)

Zitrin, A., Fabris, A., Merten, J., et al. 2015, ApJ, 801, 44,
doi: [10.1088/0004-637X/801/1/44](https://doi.org/10.1088/0004-637X/801/1/44)